2. MINERAL ASSOCIATIONS AND GEOCHEMICAL INDICATORS IN UPPER MIOCENE TO PLEISTOCENE SEDIMENTS IN THE ALBORAN BASIN[1]

Francisca Martínez-Ruíz,[2] Maria C. Comas,[2] and Belén Alonso[3]

ABSTRACT

Upper Miocene to Pleistocene hemipelagites and resedimented facies recovered at Holes 976B and 977A (Leg 161) in the Alboran Basin consist mainly of biogenic and detrital components, with a minor contribution of neoformed mineral phases. Diagenetic processes have not obliterated the primary deposition signal, and therefore detrital components (quartz, feldspar, detrital dolomite, rock fragments, and clays) provide information about source rocks and provenances. No major bulk or clay mineralogy differences were recognized between resedimented and hemipelagic facies; in fact, similar mineral assemblages in both types of facies suggest common source rocks. However, mineral abundance fluctuations can be related to climate variations and tectonic factors, as the main controls of sediment fill of this basin. A marked increase in smectites in Messinian sediments suggests an extensive development of soils during that time, probably favored by the alternation of wet and dry climate episodes and the relative aridification of the Mediterranean borderlands. A notable increase in detrital components suggests a sea-level fall and/or tectonic uplift during the late Pliocene. The significant increase in detrital dolomite in the uppermost Pliocene deposits suggests the uplift of dolomite-rich rocks as source areas. Mineral components in Pleistocene sediments indicate increasing tectonic stability, and clay-mineral fluctuations during the Pleistocene can be related not only to tectonic events, but also to alternating cooling and warming periods.

INTRODUCTION

During Ocean Drilling Program Leg 161, four sites (Sites 976–979) were drilled in the Alboran Sea basin (Fig. 1). Site 976 (1108 meters below seafloor [mbsf]), in the West Alboran Basin, lies on top of a basement horst 60 km off the southern Spanish coast and 8 km northeast of Deep Sea Drilling Project Site 121. Site 977 (1984 mbsf) is located in the East Alboran Basin, south of the Al-Mansour Seamount (Fig 1). These two sites provided information on the nature and ages of sediments located in the westernmost and easternmost regions of the Alboran Sea basin. Furthermore, drilling results shed light on paleoenvironmental behavior and the main events in sedimentary basin evolution from the Miocene to the present.

Hole 976B in the West Alboran Basin cored a 670-m-thick, middle Miocene (Serravallian) to Pleistocene/Holocene sedimentary sequence lying directly upon the metamorphic basement. Sediments consist of nannofossil clay, nannofossil silty clay, sand, silt, calcareous silty clay, and claystone. The sedimentary sequences at Site 976 were divided into four lithostratigraphic units (Units I–IV) primarily on the basis of downhole grain-size variations (Shipboard Scientific Party, 1996a). Hole 977A sampled 598.5 m of uppermost Miocene–Pleistocene/Holocene sediments consisting of nannofossil clay, and calcareous and nannofossil silty clay to clay. Sediments recovered at Site 977 were divided in two lithostratigraphic units (Units I and II) on the basis of downhole changes in sedimentary structures and sediment grain size. Unit I was subdivided into three subunits (IA–IC; Shipboard Scientific Party, 1996b). The discovery of organic-rich layers (ORLs) in the Alboran Basin was one of the major findings of Leg 161. At Site 976, ORLs were identified in the Pliocene deposits, with total organic carbon (TOC) ranging from 0.95% to 1.3%. At Site 977, ORLs were identified in the upper Pliocene–Pleistocene sequence, with an average TOC of ~0.90% (Comas, Zahn, Klaus, et al., 1996). ORLs, defined as sapropels in the eastern Mediterranean, appear in deposits from the middle Miocene and younger (e.g., Hilgen, 1991), although their origin remains controversial.

This paper analyzes mineral and geochemical compositions of sediments recovered at Holes 976B and 977A to identify source rocks and provenance of sediments, mineral origin and trends, and the influence of climatic and/or tectonic factors during sedimentary processes in the Alboran basin since the Miocene.

MATERIALS AND METHODS

Bulk and clay mineral data and bulk trace-element compositions were obtained from 400 samples from Holes 976B and 50 samples from Hole 977A. From Hole 976B, we analyzed samples from lithostratigraphic Unit I (0–362.10 mbsf), consisting of nannofossil-rich clay, nannofossil clay, and nannofossil silty clay; Unit II (362.10–518.30 mbsf), consisting of sand, silt, calcareous silty clay, and nannofossil clay; and Unit III (518.30–660.20 mbsf), comprising nannofossil-rich clay and claystone (Fig. 2). We also present data from lithostratigraphic Unit I from Hole 977A, from Subunits IA (0.0–417.4 mbsf), IB (417.4–490.6 mbsf), and IC (490.6–532.9 mbsf), made up of nannofossil clay and calcareous and nannofossil silty clay to clay (Fig. 3).

X-ray Diffraction

A representative and homogeneous part of each sample was used for bulk mineralogy and clay mineral studies. Samples were homogenized by grinding and then splitting the powder. For bulk mineralogy, samples were air dried, ground in an agate mortar to <0.0053 µm, and packed in Al sample holders for X-ray diffraction (XRD). For clay mineral analyses, the carbonate fraction was removed using acetic acid. The reaction was started at a very low acid concentration (0.1 N), and the concentration was increased to 1 N, depending on the carbonate content of each sample. Clay was deflocculated by successive washing with demineralized water after carbonate removal. The <2-µm fraction was separated by centrifugation at 9000 rpm for 1.3 min. The clay fraction was smeared onto glass slides for XRD. Separation

[1]Zahn, R., Comas, M.C., and Klaus, A. (Eds.), 1999. *Proc. ODP, Sci. Results*, 161: College Station, TX (Ocean Drilling Program).

[2]Instituto Andaluz de Ciencias de la Tierra (CSIC-University of Granada), Campus Fuentenueva, 18002 Granada, Spain. fmruiz@goliat.ugr.es

[3]Instituto de Ciencias del Mar (CSIC), Paseo Joan de Borbo s/n 08039 Barcelona, Spain.

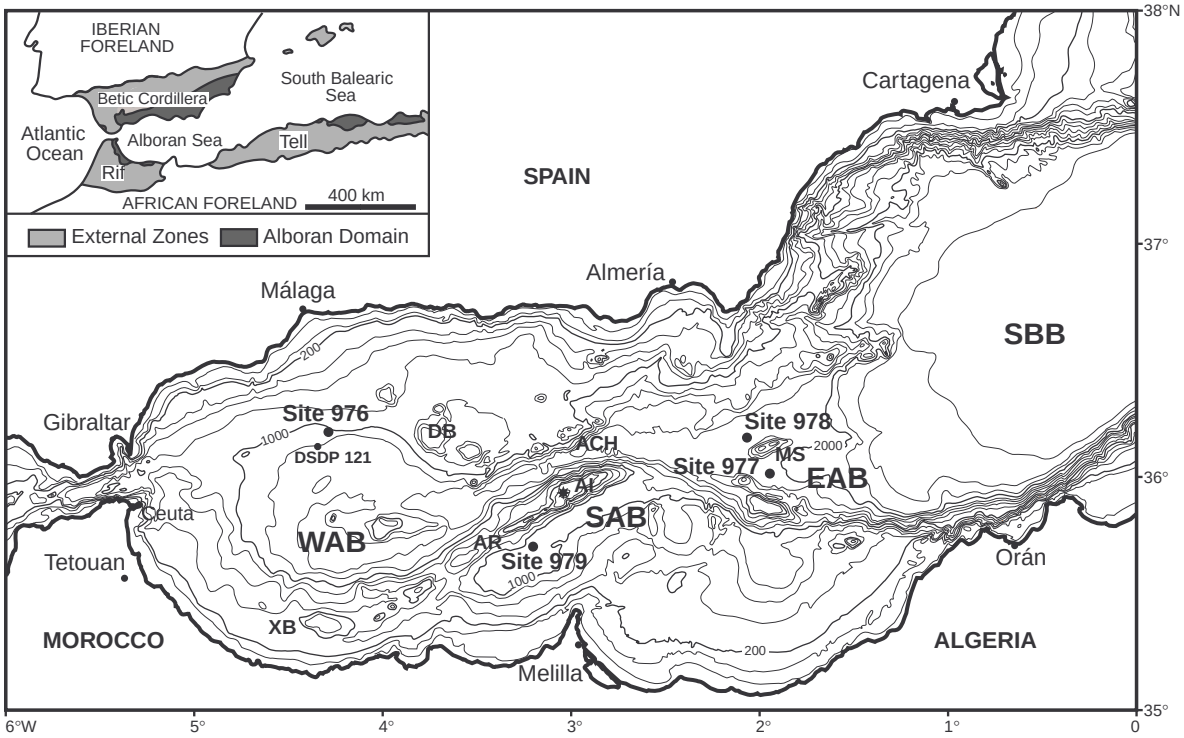

Figure 1. Bathymetric map of the Alboran Sea showing the location of Leg 161 sites. The inset map shows the location of the Alboran Sea between the Betic and Rif Cordilleras and the general tectonic subdivisions. Contour lines are in meters. EAB = East Alboran Basin, WAB = West Alboran Basin, SAB = South Alboran Basin, AR = Alboran Ridge, AI = Alboran Island, ACH = Alboran Channel, MS = Al-Mansour Seamount, XB = Xauen Bank, DB = Djibouti Bank.

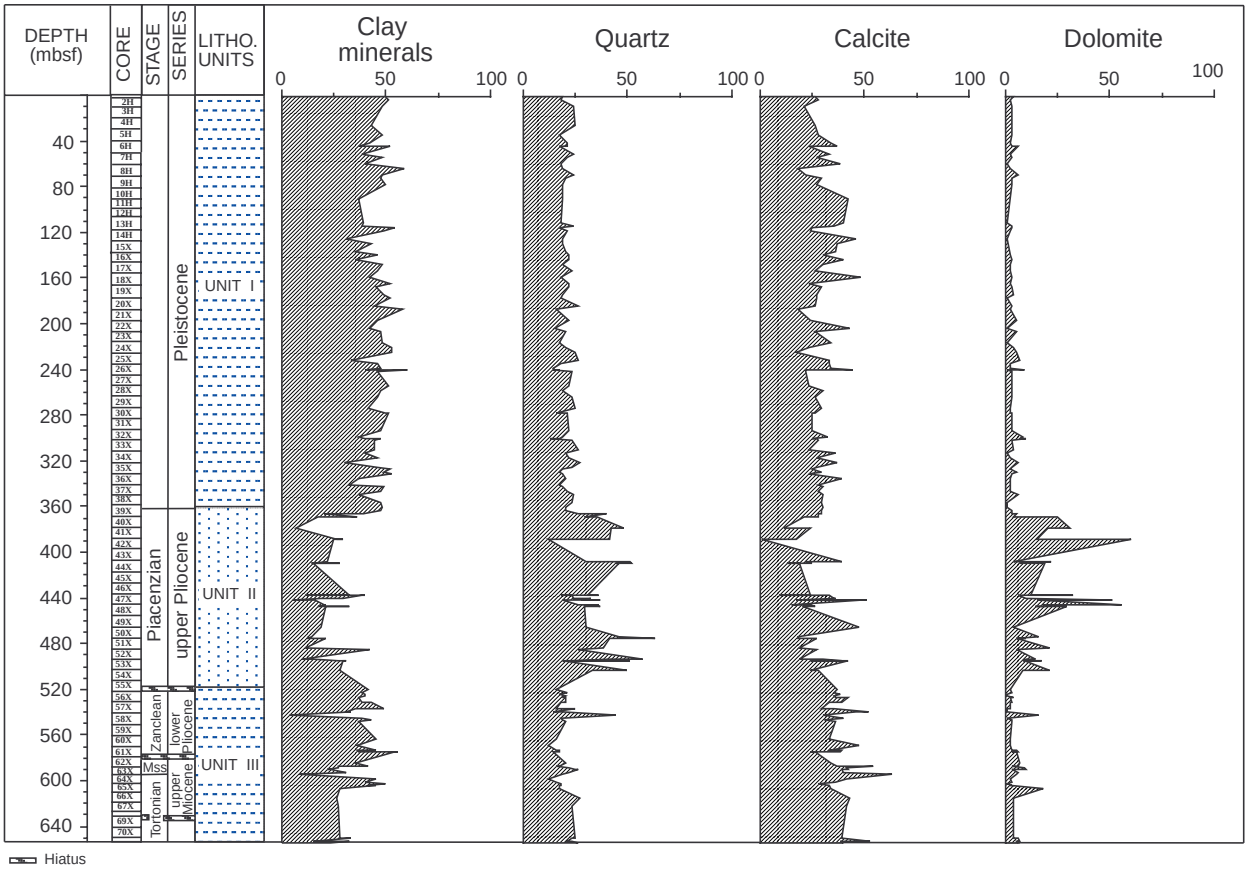

Figure 2. Bulk mineralogy, Hole 976B.

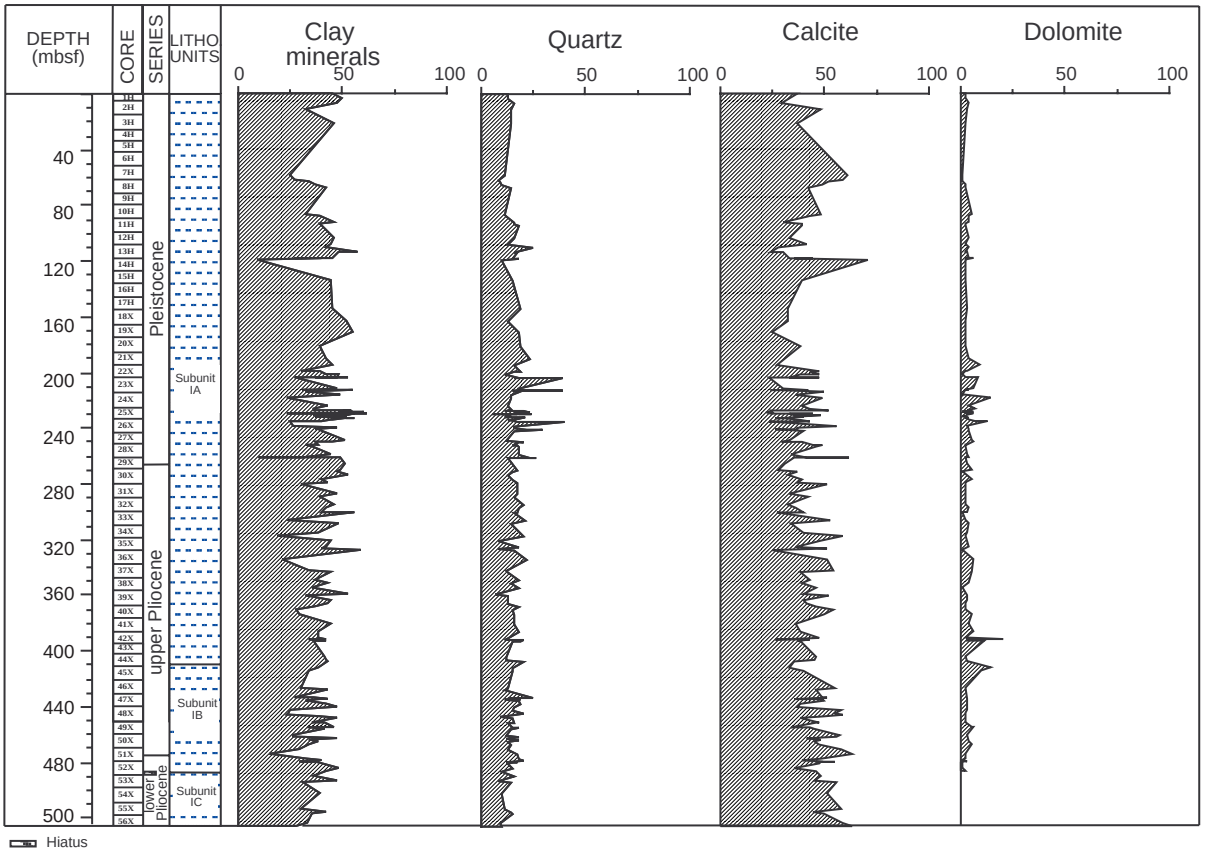

Figure 3. Bulk mineralogy, Hole 977A.

of the clay fraction and preparation of the samples for XRD were performed following the international recommendations compiled by Kisch (1991). X-ray diffractograms were obtained using a Philips PW 1710 diffractometer with Cu-Kα radiation and automatic slit. Scans were run from 2°–64° 2θ for bulk-sample diffractograms and untreated clay preparations, and from 2°–30° 2θ for glycolated and heated (550°C) clay-fraction samples. The reflecting factors calculated for this equipment and its instrument conditions were (1) for powder diffractograms: phyllosilicates, 0.09; quartz, 1.43; calcite, 1.05; feldspar, 1.03; (2) for oriented sample diffractograms: illite, 0.36; chlorite, kaolinite, 0.98; I/S mixed-layer, 0.65. Diffractograms were visually interpreted with the help of a computerized search. Semiquantitative analyses were performed considering the integrated peak area using a computer program specific for the diffractometer used. The clay mineral proportion was estimated from the glycolated diffractogram. The 10-Å peak was used for illite, and the 7-Å peak for the total amount of chlorite + kaolinite, using the peak ratios at 3.54 Å and 3.58 Å, respectively, to differentiate these minerals. The 17-Å peak was used for smectites, and the area between the illite peak at 10 Å and the smectite peak at 17 Å was used in some cases to estimate the proportion of mixed layers. We did not estimate the relative percentage of illite/smectite (I/S) mixed layers because the peaks were usually masked by smectite and illite peaks. The estimated semiquantitative analysis error for bulk mineralogy absolute values is 5%; for clay mineral proportions, error ranges from 5% to 10%. Note that the main value of semiquantitative analysis is to show changes or gradients in mineral abundances, rather than absolute values.

Electron Microscopy

Morphological studies on selected samples were performed using scanning electron microscopy (SEM; Zeiss DSM 950), whereas quantitative geochemical microanalyses of the clay minerals were obtained by transmission electron microscopy (TEM) using a Philips CM-20 equipped with an EDAX microanalysis system (Instrument Services of the University of Granada, Spain). Quantitative analyses were obtained in scanning TEM mode only from the edges using a 70-Å diameter beam and 200 × 1000 Å scanning area. To avoid alkali loss, which is a significant problem in clay mineral analyses (Van der Pluijm et al., 1988), we used a short counting time (30 s), which provides better reproducibility for alkali contents (Nieto et al., 1996). The formulae of micas, smectites, and I/S mixed layers were normalized to 11 oxygens, and that of chlorite was normalized to 14 oxygens.

Chemical Analyses

Analyses of trace elements in bulk samples were performed by inductively coupled plasma-mass spectrometry (ICP-MS) after HNO_3 + HF digestion of 0.1000 g of sample powder in a Teflon-lined vessel for 150 min at high temperature and pressure, evaporation to dryness, and subsequent dissolution in 100 ml of 4 vol% HNO_3. Measurements were performed in triplicate using a Perkin Elmer Sciex Elan 5000 spectrometer (Instrument Services of the University of Granada, Spain), with Re and Rh as internal standards. Coefficients of variation calculated by dissolution and subsequent analyses of 10 replicates of powdered samples were better than +3 (rel%) and +8 (rel%) for analyte concentrations of 50 and 5 ppm, respectively (Bea, 1996).

RESULTS

Bulk Mineralogy: Holes 976B and 977A

XRD analyses demonstrated that the studied sediments are mainly composed of clay minerals, calcite, quartz, and dolomite, with trace amounts of feldspar and pyrite. Previous work in sediments from Site

121 (Dunoyer de Segonzac and Hoffert, 1973; Nesteroff, 1973; Zemmels and Cook, 1973) revealed mineral associations similar to those reported here for the samples from Hole 976B (Fig. 1).

Bulk mineralogy semiquantitative results for Hole 976B indicate the following ranges:

1. Unit I: calcite 20%–50%, dolomite <5%, quartz 15%–25%, clay minerals 40%–60%;
2. Unit II: calcite 15%–35%, dolomite 5%–60%, quartz 15%–60%, clay minerals 10%–40%; and
3. Unit III: calcite 25%–60%, dolomite <5%, quartz 15%–25%, clay minerals 40%–50%.

Proportions of the major components for each sample are listed in Table 1 and illustrated in Figure 2. Minor components are feldspar and pyrite. Apatite, zircon, biotite, and garnet are the main accessory minerals in the coarser fraction. Bulk mineralogy data indicate that Unit III (from Section 976B-56X-1, 0 cm, to 72X-1, 0 cm) is richer in calcite than the other lithostratigraphic units from this hole. The lower part of Unit II (Cores 976B-48X through 56X) is richer in quartz, whereas the upper part is richer in dolomite (Cores 976B-39X through 48X), and Unit I (from Section 976B-1H-1, 0 cm, to 39X-3, 144 cm) is richer in clays (Fig. 2).

Semiquantitative results for Hole 977A indicate the following ranges:

1. Subunit IA: calcite 25%–70%, dolomite <5%–15%, quartz 10%–40%, clay minerals 10%–60%;
2. Subunit IB: calcite 30%–60%, dolomite <5%–15%, quartz 10%–25%, clay minerals 15%–50%; and
3. Subunit IC: calcite 50%–60%, dolomite <5%, quartz 10%–15%, clay minerals 30%–40%.

Detailed proportions of the major components for each sample are listed in Table 2 and illustrated in Figure 3. Minor components are feldspar and pyrite. Apatite, zircon, biotite, and garnet are once again the main accessory minerals in the coarser fraction. The mineral composition is generally more uniform than in Hole 976B. No significant variations are observed among the different subunits, except that Subunit IA (from Section 977A–1H, 0 cm, to 45X-2, 32 cm) contains some intervals richer in quartz than either Subunit IB (from Section 977A-45X-2, 32 cm, to 52X-6, 21 cm) or Subunit IC (from Section 977A-52X-6, 21 cm, to 57X-CC, 46 cm).

SEM investigations of these sediments at both holes reveal that the fine-grained material mainly consists of clay minerals (Pl. 1, fig. 1) and biogenic components (Pl. 1, fig. 2). Quartz, feldspar, and micas are detrital grains, and quartz morphology varies from rounded to angular grains (Pl. 1, figs. 3, 4). Calcite is mainly biogenic in origin (Pl. 1, fig. 2), although some inorganic calcite also occurs. Dolomites occur as detrital grains (up to 50 µm), and euhedral dolomite crystals smaller than 10 µm are embedded in the clayey matrix and associated with weakly cemented beds (Pl. 1, figs. 4, 6). Pyrite occurs disseminated mainly as framboids, although small cubic crystals and irregular particles that may have replaced organic fragments are also present.

Upper Miocene and lower Pliocene sediments at Hole 976B show a similar bulk-mineral composition. In the upper Pliocene sediments, we noted a significant increase in the quartz and dolomite, whereas no meaningful variations were observed in the Pleistocene deposits. Pliocene and Pleistocene sediments at Hole 977A show a relatively uniform bulk-mineral composition with only short-term fluctuations.

Clay Mineralogy: Holes 976B and 977A

The clay mineral assemblages in sediment samples from Holes 976B and 977A are mainly composed of illite, smectite, chlorite, and kaolinite. Relative percentages of these minerals are shown in Tables 3 and 4 and illustrated in Figure 3 for Hole 976B.

Semiquantitative results from Hole 976B indicate relative changes in the following ranges:

1. Unit I: smectites 5%–25%, illite 40%–70%, kaolinite 5%–25%, and chlorite 10%–25%;
2. Unit II: smectites <5%–15%, illite 60%–80%, kaolinite 5%–15%, and chlorite 10%–25%; and
3. Unit III: smectites 10%–80%, illite 10%–60%, kaolinite <5%–20%, and chlorite <5%–20%.

Following are semiquantitative results from Hole 977A:

1. Unit I: smectites <5%–40%, illite 35%–70%, kaolinite 5%–20%, and chlorite 5%–20%.

These results indicate that illite is the most abundant clay mineral in upper Pliocene/Pleistocene sediments from Holes 976B (Units I and II) and 977A (Subunits IA, IB, and IC), followed by smectite and kaolinite + chlorite. In contrast to Pliocene and Pleistocene deposits, the uppermost Miocene sediments at Hole 976B (Unit III) are characterized by a higher smectite content.

The clay mineral associations at Hole 976B (Fig. 4) are varied. In Unit III, which is richer in calcite, two different trends are recognized for clay minerals: increasing smectite is associated with a decrease in kaolinite and chlorite (from 610 to 550 mbsf, upper Miocene), and decreasing smectite is associated with an increase in kaolinite, chlorite, and illite (from 550 to 520 mbsf, lower Pliocene). In Unit II (upper Pliocene), where two different bulk-mineral assemblages are recognized (quartz-rich and dolomite-rich levels), the clay mineral abundance is more homogeneous. In Unit I (Pleistocene), richer in clay, results indicate a slight increase in kaolinite (from 156 to 0 mbsf), with a decrease in illite (from 50 to 0 mbsf) in the uppermost Pleistocene deposits, although the abundance values for different samples fluctuate. Smectite shows a slight but continuous increase from the bottom of this unit up to 150 mbsf, with a pronounced increase between 100 and 150 mbsf. From this interval to the top of this unit, four more intervals are distinguished on the basis of smectite content: 100–150 mbsf with a lower smectite content; 70–100 with a higher smectite content; 40–70 mbsf with a lower smectite content, and 0–40 mbsf with smectite content increasing to the top of the hole (Fig. 4). Minor amounts of illite/smectite (I/S) mixed layers and fibrous clays (palygorskite and sepiolite) are recognized in clay mineral assemblages in most of the samples. In addition, fibrous clays are scattered throughout sediments from both holes.

No major qualitative changes in clay minerals were detected among the types of sedimentary facies in samples from either hole. Quantitatively, the most significant change in clay mineral content occurs in Messinian sediments, as indicated by a sharp increase in smectite content (Fig. 4).

Microchemical analyses of clay minerals revealed that smectite composition corresponds to Al-rich beidellites (Tables 5–7; Fig. 5) and illite corresponds to detrital mica, which is also corroborated by the morphological characterization of these micas by SEM (Pl. 1, fig. 4).

Effects of diagenesis on clay mineral assemblages are negligible. Furthermore, as there is no consistent increase with depth of I/S mixed layers, diagenesis cannot account for the origin of these minerals.

Trace-Element Geochemistry

Figures 6 and 7 (see also Tables 8 and 9) summarize the ICP-MS results from Hole 976B and 977A samples. Preliminary geochemical studies of Sr, Ba, REEs, Rb, and Cu content indicate some variations of these elements as a function of facies and stratigraphic ages.

Table 1. Bulk mineral composition for Hole 976B.

Core, section, interval (cm)	Depth (mbsf)	Phyllosilicates (%)	Quartz (%)	Calcite (%)	Dolomite (%)
161-976B-					
1H-1, 15-19	0.15	50	19	26	<5
1H-2, 130-134	2.80	51	18	28	<5
2H-4, 32-36	8.32	48	24	21	<5
2H-6, 6-11	11.06	41	36	22	<5
4H-2, 30-32	24.80	43	25	26	<5
5H-2, 30-32	33.80	48	17	28	<5
5H-6, 90-92	40.40	42	21	34	<5
6H-1, 118-123	42.68	37	21	37	<5
6H-2, 31-32	43.31	52	17	23	6
6H-6, 90-92	49.90	38	24	33	<5
7H-2, 30-32	52.80	48	21	27	<5
7H-6, 90-92	59.40	40	18	38	<5
8H-2, 30-35	62.30	59	19	18	<5
8H-6, 90-95	68.90	48	24	22	<5
9H-2, 31-36	70.81	47	20	29	<5
9H-5, 122-127	77.27	50	19	27	<5
11H-2, 30-35	89.40	36	19	42	<5
13H-2, 30-35	109.80	39	18	40	<5
13H-4, 94-99	113.44	38	24	35	<5
13H-5, 90-95	114.90	54	17	25	<5
14H-2, 31-35	118.06	49	21	24	<5
14H-6, 90-95	124.45	31	19	46	<5
15X-2, 30-36	128.80	42	19	37	<5
15X-6, 90-95	135.40	34	20	36	<5
16X-2, 30-34	138.30	46	22	30	<5
16X-4, 120-125	142.20	35	22	40	<5
17X-2, 30-34	147.50	48	19	30	<5
17X-6, 90-94	153.10	46	23	26	<5
18X-2, 30-32	157.60	42	18	38	<5
18X-6, 90-92	164.20	52	22	23	<5
19X-2, 30-32	166.93	45	22	29	<5
19X-6, 90-92	173.53	49	19	27	<5
20X-2, 31-33	176.91	52	18	27	<5
20X-6, 90-92	183.50	44	26	26	<5
21X-2, 30-32	186.40	58	16	18	<5
22X-2, 30-35	196.20	46	22	24	<5
22X-6, 90-95	202.80	41	15	41	<5
23X-2, 30-35	205.70	47	20	26	5
24X-2, 30-34	215.30	48	17	34	<5
24X-5, 76-80	220.26	53	20	23	<5
25X-2, 31-33	223.71	53	25	17	5
25X-6, 90-92	230.50	33	26	33	7
26X-2, 64-68	233.89	46	18	33	<5
26X-4, 121-125	237.46	47	14	34	<5
26X-6, 12-14	238.78	40	15	40	5
26X-6, 52-56	239.18	51	17	27	5
26X-6, 61-65	239.27	60	14	22	<5
26X-7, 13-18	240.29	46	23	22	<5
28X-2, 73-78	253.23	51	22	23	<5
28X-5, 78-83	257.78	47	19	30	<5
29X-2, 73-75	262.83	46	23	26	<5
30X-2, 73-79	272.89	41	25	29	<5
30X-5, 25-27	276.56	50	16	26	<5
30X-5, 77-82	277.08	51	21	25	<5
32X-2, 70-72	291.70	47	22	25	<5
32X-6, 38-40	297.23	37	19	32	8
32X-7, 50-54	298.85	40	17	25	7
32X-7, 74-76	299.09	47	13	27	10
33X-2, 72-77	301.24	44	23	28	<5
33X-7, 60-65	308.47	44	26	23	<5
34X-2, 33-35	311.26	40	20	36	<5
34X-5, 91-95	316.34	46	22	27	<5
35X-2, 32-34	320.82	30	27	37	6
35X-5, 25-27	325.12	46	23	27	<5
35X-5, 91-98	325.78	52	19	25	<5
35X-7, 61-65	328.38	49	17	29	5
36X-2, 33-39	329.63	53	19	23	<5
36X-5, 92-98	334.12	37	20	39	<5
37X-2, 33-40	339.73	42	19	35	<5
37X-3, 66-68	341.52	49	19	30	<5
37X-5, 92-100	344.81	47	21	28	<5
38X-2, 33-35	348.93	37	24	30	6
38X-5, 92-94	355.02	47	23	29	<5
39X-2, 33-38	359.53	48	20	30	<5
39X-4, 35-37	362.55	47	20	29	<5
39X-5, 90-95	364.60	39	26	29	<5
39X-CC, 17-19	364.82	30	40	28	5
40X-1, 43-45	367.83	36	29	28	<5
40X-CC, 33-35	368.23	17	35	21	25
41X-CC, 5-7	377.05	74	8	11	31
41X-CC, 21-23	377.21	74	2	24	20
42X-CC, 21-23	386.81	26	41	17	15
42X-CC, 25-27	386.85	29	13	<5	55
42X-CC, 28-30	386.88	25	12	<5	59
44X-1, 103-105	406.93	25	33	39	<5
44X-2, 13-15	407.53	<5	51	22	22
44X-2, 33-38	407.73	14	52	25	7
44X-2, 52-54	407.92	28	44	13	12
44X-CC, 10-12	408.12	15	46	19	19
47X-2, 21-23	436.51	32	31	24	12
47X-2, 29-31	436.59	11	36	19	30
47X-2, 33-35	436.63	28	27	9	32
47X-2, 38-40	436.68	40	18	33	6
47X-2, 41-45	436.71	38	23	33	6
47X-3, 145-147	439.25	29	24	35	10
47X-4, 2-4	439.32	19	32	36	10
47X-4, 73-75	440.03	<5	28	17	51
47X-4, 76-78	440.06	<5	29	51	16
47X-CC, 2-4	440.17	53	7	21	35
47X-CC, 5-8	440.20	16	19	49	15
48X-1, 23-25	444.73	<5	26	15	56
48X-1, 60-62	445.10	20	36	24	18
48X-1, 64-66	445.14	21	30	24	21
48X-2, 9-11	446.09	17	37	26	19
48X-2, 33-35	446.33	32	33	20	14
48X-2, 40-42	446.40	21	29	20	29
50X-CC, 6-10	463.76	19	30	47	<5
51X-1, 9-11	473.39	14	46	18	16
51X-1, 66-68	473.96	12	63	18	5
51X-1, 72-74	474.02	18	44	25	10
51X-1, 83-85	474.13	21	41	27	5
52X-1, 9-11	482.89	11	38	19	21
52X-1, 42-44	483.22	42	26	27	5
53X-1, 9-11	492.49	10	57	19	14
53X-1, 15-17	492.55	15	41	30	10
53X-1, 76-78	493.16	27	23	38	<5
53X-1, 92-94	493.32	31	25	36	8
53X-2, 6-8	493.96	<5	51	24	17
53X-CC, 18-20	494.37	29	19	42	9
54X-1, 27-29	502.27	<5	50	24	21
54X-1, 45-47	502.45	28	33	28	8
56X-1, 47-49	518.77	41	16	37	<5
56X-3, 72-74	521.25	38	21	35	<5
56X-4, 47-49	522.50	40	17	38	<5
56X-5, 108-110	524.61	40	20	35	<5
56X-7, 113-115	526.02	37	19	36	<5
57X-1, 92-94	526.22	37	20	42	<5
57X-3, 143-145	529.73	38	20	39	<5
57X-4, 45-47	530.25	43	18	33	<5
58X-1, 45-47	535.35	49	16	29	<5
58X-1, 51-53	535.41	35	25	35	<5
58X-3, 92-94	537.88	31	14	52	<5
58X-3, 108-110	538.03	33	19	46	<5
58X-5, 79-81	540.74	<5	44	30	16
58X-8, 47-49	544.37	38	18	40	<5
59X-2, 2-4	546.12	43	19	31	<5
59X-2, 8-10	546.18	37	20	36	<5
60X-6, 120-123	561.72	45	16	33	<5
61X-4, 66-75	567.93	36	12	47	<5
61X-6, 125-123	571.52	45	16	33	<5
61X-7, 23-25	571.87	36	17	39	<5
61X-8, 8-10	573.22	37	17	38	<5
61X-CC, 17-19	573.82	54	14	26	5
62X-CC, 5-8	573.55	56	14	24	<5
63X-1, 50-54	583.60	35	20	34	7
63X-2, 74-79	585.34	41	17	37	6
63X-3, 56-59	586.66	27	16	54	<5
63X-4, 40-42	588.00	27	22	41	9
63X-4, 68-71	588.28	22	25	42	10
63X-4, 76-78	588.36	23	26	39	<5
63X-6, 123-126	591.83	31	22	40	6
64X-1, 32-34	593.12	81	9	63	5
64X-4, 56-58	597.86	45	12	41	<5
64X-5, 113-115	599.93	40	16	36	<5
64X-6, 43-45	600.73	50	18	28	<5
64X-7, 55-57	602.25	41	18	33	<5
64X-CC, 18-20	602.48	45	17	33	<5
65X-2, 145-147	605.15	28	17	34	18
66X-3, 59-61	614.39	26	27	43	<5
66X-8, 43-46	621.43	27	23	41	<5
70X-6, 30-32	648.70	28	25	39	<5
70X-7, 16-18	649.26	33	23	39	6
71X-1, 87-89	651.37	32	23	38	5
71X-2, 15-17	651.15	15	21	53	7
71X-3, 14-16	653.14	23	26	40	6

Note: X-ray diffraction data (%).

Table 2. Bulk mineral composition for Hole 977A.

Core, section, interval (cm)	Depth (mbsf)	Phyllosilicates (%)	Quartz (%)	Calcite (%)	Dolomite (%)
161-977A-					
1H-1, 29-34	0.32	45	13	37	<5
1H-3, 64-69	3.50	50	13	33	<5
2H-2, 92-97	6.35	47	16	29	<5
2H-5, 79-84	11.20	32	14	48	<5
3H-6, 4-9	21.04	46	14	37	<5
6H-5, 80-84	58.20	25	11	61	<5
7H-1, 72-74	61.80	27	85	9	<5
7H-5, 80-85	63.20	34	95	2	<5
8H-2, 80-85	65.50	37	10	49	<5
8H-5, 83-88	67.12	42	14	42	<5
9H-5, 14-18	86.00	32	11	48	<5
10H-5, 80-86	88.00	39	12	43	<5
11H-2, 132-134	92.00	46	16	30	<5
11H-3, 3-5	93.00	39	16	39	<5
11H-4, 122-127	94.00	40	18	39	<5
12H-3, 79-84	103.00	46	16	32	<5
13H-1, 9-14	108.00	44	13	40	<5
13H-3, 114-116	110.00	42	25	27	<5
13H-4, 33-35	113.00	57	16	23	<5
13H-4, 126-128	113.70	48	17	30	<5
13H-7, 10-12	117.60	45	15	33	<5
13H-7, 58-60	118.00	27	15	44	<5
14H-1, 14-16	118.14	40	18	35	6
14H-1, 98-100	119.00	9	71	10	<5
15H-5, 6-8	133.56	44	15	39	<5
17H-6, 27-29	154.27	45	19	32	<5
18X-5, 102-104	163.02	52	13	32	<5
19X-5, 26-28	170.36	55	18	25	<5
20X-4, 97-99	180.67	39	19	38	<5
21X-3, 145-147	189.35	42	23	31	<5
21X-7, 19-21	194.09	45	16	27	9
22X-4, 3-5	198.93	30	19	47	<5
22X-4, 28-30	199.18	39	16	43	<5
22X-5, 10-12	200.50	42	11	46	<5
22X-5, 63-65	201.03	48	12	38	<5
22X-7, 7-9	203.48	47	18	33	<5
22X-7, 11-13	203.51	37	16	46	<5
22X-7, 25-27	203.65	53	18	26	<5
22X-7, 31-33	203.71	27	39	23	8
23X-5, 55-57	210.55	47	17	30	6
23X-6, 47-49	211.97	36	20	42	<5
23X-6, 73-75	212.23	31	39	24	<5
23X-6, 90-92	212.40	51	15	29	<5
23X-6, 145-146	212.95	32	18	49	<5
24X-2, 40-42	215.50	49	14	36	<5
24X-3, 89-91	217.49	23	14	49	14
25X-1, 48-50	223.68	43	13	39	<5
25X-2, 77-83	225.50	36	14	43	7
25X-3, 4-6	226.27	36	12	51	<5
25X-3, 22-24	226.45	44	11	44	<5
25X-3, 63-65	226.86	54	12	31	<5
25X-3, 101-103	227.24	52	20	24	<5
25X-3, 114-116	227.37	48	23	25	<5
25X-3, 128-130	227.51	53	16	25	6
25X-4, 26-28	227.99	55	19	25	<5
25X-4, 40-42	228.13	53	17	23	5
25X-4, 65-67	228.38	60	16	22	<5
25X-4, 79-81	228.52	54	18	24	<5
25X-4, 79-81	228.52	54	18	24	<5
25X-4, 83-88	228.56	49	24	25	<5
25X-4, 102-104	228.75	62	52	6	<5
25X-4, 116-118	228.89	51	13	33	<5
25X-4, 134-136	229.07	23	17	44	6
25X-4, 147-149	229.20	56	11	32	<5
25X-5, 68-70	229.91	53	12	34	<5
25X-5, 115-117	230.38	44	13	40	<5
25X-5, 132-134	230.55	36	14	47	<5
25X-6, 31-33	231.04	50	11	36	<5
25X-6, 78-80	231.51	44	17	38	<5
25X-6, 92-93	231.65	37	21	40	<5
25X-6, 132-137	232.07	52	18	26	<5
25X-7, 24-26	232.47	56	16	26	<5
25X-CC, 3-5	232.75	51	18	30	<5
25X-CC, 33-34	233.05	45	13	38	<5
26X-1, 51-53	233.41	44	14	38	<5
26X-1, 135-137	234.25	40	17	42	<5
26X-2, 2-4	234.42	30	32	31	7
26X-2, 7-9	234.47	25	38	23	13
26X-4, 83-87	238.23	26	16	54	<5
26X-5, 26-28	239.16	47	16	36	<5
26X-5, 135-137	240.25	37	22	37	<5
26X-6, 3-5	240.43	38	29	25	<5
26X-6, 132-136	241.72	40	16	40	<5
27X-4, 84-89	247.94	49	12	33	<5
27X-5, 11-13	248.71	45	20	29	6
27X-5, 50-52	249.10	37	18	39	6
27X-6, 108-110	251.18	38	15	44	<5
27X-6, 140-142	251.50	32	17	49	<5
28X-1, 82-84	253.02	35	18	44	<5
28X-4, 82-88	257.72	44	18	34	<5
28X-6, 28-30	259.95	31	23	41	<5
28X-6, 69-71	260.36	10	26	62	<5
28X-6, 130-135	260.95	49	13	35	<5
29X-2, 142-144	264.72	51	15	31	<5
29X-5, 113-115	268.93	49	17	28	5
29X-6, 131-136	270.61	47	15	37	<5
30X-2, 27-29	273.17	53	13	31	<5
30X-4, 83-89	276.73	40	15	39	5
30X-6, 4-6	278.94	43	17	37	<5
30X-6, 79-81	279.69	30	17	51	<5
31X-4, 82-88	286.32	47	17	33	<5
31X-5, 135-140	288.35	39	16	42	<5
32X-3, 65-67	294.15	46	20	32	<5
32X-4, 135-137	296.35	42	18	36	<5
32X-6, 122-129	299.22	40	17	40	<5
32X-7, 49-51	299.99	56	16	27	<5
33X-4, 71-74	305.32	23	21	53	<5
33X-6, 132-134	307.32	48	14	34	<5
34X-4, 71-73	314.91	38	19	40	<5
34X-6, 138-140	316.58	19	20	59	<5
35X-1, 7-9	319.47	44	84	7	<5
35X-4, 61-63	324.51	42	18	36	<5
35X-5, 62-64	326.02	40	8	50	<5
35X-6, 127-129	327.17	57	16	25	<5
36X-4, 53-55	333.93	21	22	51	6
37X-2, 92-94	340.92	34	12	53	<5
37X-3, 75-77	342.17	44	13	38	5
37X-7, 10-12	347.50	37	18	42	<5
38X-2, 34-36	350.04	43	14	39	<5
38X-4, 142-143	354.12	35	18	46	<5
39X-1, 126-127	358.16	53	7	39	<5
39X-2, 36-40	359.76	32	13	52	<5
39X-4, 27-29	362.67	44	13	40	<5
39X-5, 85-89	364.75	43	13	41	<5
39X-7, 42-44	367.32	37	18	46	<5
40X-2, 52-56	369.52	28	15	54	<5
40X-4, 36-40	372.50	29	16	50	5
41X-2, 49-51	379.09	44	16	36	<5
41X-6, 101-103	385.56	40	18	38	6
42X-3, 67-69	390.37	42	11	26	20
42X-3, 115-117	390.85	34	20	43	<5
42X-4, 9-11	391.29	40	19	37	<5
42X-4, 86-88	392.06	36	15	38	11
43X-2, 87-92	389.07	38	13	47	<5
43X-5, 74-79	403.14	40	12	45	<5
44X-5, 101-103	404.91	42	12	42	<5
45X-1, 26-28	406.26	43	20	35	<5
45X-4, 39-41	410.89	38	15	33	14
45X-5, 80-82	412.80	34	15	40	10
46X-1, 10-12	425.40	30	13	55	<5
46X-1, 135-137	426.65	43	11	45	<5
46X-5, 54-56	431.84	27	25	48	<5
46X-5, 109-111	432.39	36	13	50	<5
46X-6, 27-29	433.07	43	19	35	<5
46X-6, 75-77	433.55	40	11	48	<5
46X-6, 148-150	434.28	32	18	49	<5
47X-2, 32-34	436.72	42	19	36	<5
47X-3, 141-143	439.31	47	16	36	<5
47X-5, 59-61	441.49	25	15	56	<5
47X-6, 108-110	443.48	24	20	53	<5
48X-1, 26-28	444.76	23	15	59	<5
48X-1, 130-132	445.80	38	9	50	<5
48X-2, 54-56	446.54	47	15	37	<5
48X-4, 140-142	450.40	35	16	47	<5
48X-5, 10-12	450.60	41	13	45	<5
48X-6, 105-107	453.05	46	15	34	<5
48X-7, 9-10	453.59	33	18	43	5
49X-1, 25-27	454.35	41	14	44	6
49X-3, 41-43	460.92	47	12	40	<5
49X-4, 73-75	459.33	26	12	57	<5
49X-5, 53-55	460.63	26	18	55	<5
49X-6, 88-90	462.48	34	18	47	<5
49X-7, 15-17	463.25	38	13	45	4
50X-2, 30-34	465.50	34	14	47	5
50X-4, 80-82	469.00	29	13	57	<5
50X-7, 27-31	472.97	15	17	63	<5
51X-3, 23-25	476.53	32	18	48	<5
51X-3, 55-57	476.85	40	20	39	<5
51X-3, 145-147	477.75	35	12	50	<5
51X-4, 23-25	478.03	29	15	55	<5
51X-4, 78-80	478.58	33	17	46	<5
51X-4, 100-102	478.80	37	15	46	<5
51X-4, 140-142	479.20	40	13	46	<5
52X-1, 24-26	483.14	48	15	35	<5
52X-2, 70-72	485.10	42	10	46	<5
52X-4, 99-101	488.39	36	16	47	<5

Table 2 (continued).

Core, section, interval (cm)	Depth (mbsf)	Phyllosilicates (%)	Quartz (%)	Calcite (%)	Dolomite (%)
52X-7, 41-43	492.31	47	8	44	<5
53X-1, 36-38	492.86	31	14	55	<5
54X-6, 90-92	500.90	39	10	50	<5
55X-1, 50-52	512.30	30	11	57	<5
55X-2, 48-50	513.78	42	14	43	<5
55X-3, 93-95	515.73	35	15	49	<5
56X-1, 26-28	521.66	33	9	58	<5
56X-2, 141-145	524.31	28	10	61	<5

Note: X-ray diffraction data (%).

Table 3. Hole 976B clay mineral abundances from X-ray diffraction data.

Core, section, interval (cm)	Depth (mbsf)	Smectites (%)	Illite (%)	Kaolinite (%)	Chlorite (%)
161-976B-					
1H-1, 15-19	0.15	20	48	19	13
1H-2, 130-134	2.80	21	48	14	16
2H-1, 50-52	4.00	13	41	23	23
2H-4, 32-36	8.32	11	46	18	25
2H-6, 6-11	11.06	13	52	21	16
3H-2, 30-32	14.30	15	45	20	20
4H-2, 30-32	24.80	13	53	15	13
4H-6, 90-92	31.40	17	59	13	10
5H-2, 30-32	33.80	10	51	17	22
5H-6, 90-92	40.40	10	59	16	14
6H-1, 118-123	42.68	6	55	20	20
6H-2, 31-32	43.31	9	52	19	20
6H-6, 90-92	49.90	6	65	10	17
7H-2, 30-32	52.80	7	69	14	10
7H-4, 118-123	56.68	5	71	14	10
7H-6, 90-92	59.40	8	59	18	15
8H-6, 90-95	68.90	8	48	22	22
9H-2, 31-36	70.81	7	61	12	18
10H-2, 30-35	81.30	12	49	16	22
10H-6, 90-95	87.90	11	57	16	16
11H-2, 30-35	89.40	13	60	13	14
12H-2, 30-32	100.30	16	59	12	12
12H-6, 90-92	107.90	<5	57	20	19
13H-2, 30-35	109.80	6	62	15	17
13H-4, 94-99	113.44	8	59	15	19
13H-5, 90-95	114.90	10	46	20	25
14H-6, 90-95	124.45	5	65	18	12
15X-2, 30-36	128.80	10	52	17	15
15X-6, 90-95	135.40	12	65	10	13
16X-4, 120-125	142.20	8	48	20	24
17X-2, 30-34	147.50	11	49	16	20
17X-6, 90-94	153.10	21	52	10	15
20X-2, 31-33	176.91	23	58	12	12
21X-2, 30-32	186.40	24	46	12	9
22X-2, 30-35	196.20	21	57	10	12
22X-6, 90-95	202.80	10	66	13	10
23X-2, 30-35	205.70	12	60	11	19
24X-2, 30-34	215.30	12	52	18	18
24X-5, 76-80	220.26	14	44	21	21
25X-2, 31-33	223.71	14	62	15	10
25X-6, 90-92	230.50	18	65	11	14
26X-2, 64-68	233.89	10	64	10	14
26X-5, 78-83	238.53	16	60	10	14
28X-2, 73-78	253.23	11	57	12	13
28X-5, 78-83	257.78	12	63	10	15
29X-2, 73-75	262.83	14	64	8	14
29X-7, 73-75	269.62	9	59	10	16
30X-2, 73-79	272.89	10	55	14	13
30X-5, 25-27	276.56	9	70	12	9
30X-5, 77-82	277.08	11	65	10	13
32X-2, 70-72	291.70	9	64	17	23
32X-6, 38-40	297.23	10	51	17	21
32X-7, 50-54	298.85	15	63	11	11
32X-7, 74-76	299.09	10	67	10	13
33X-2, 72-77	301.24	12	63	13	12
33X-7, 60-65	308.47	10	55	16	19
34X-5, 91-95	316.34	<5	68	10	18
35X-2, 32-34	320.82	<5	62	15	19
35X-5, 25-27	325.12	<5	78	6	14
35X-5, 91-98	325.78	<5	78	9	9
35X-7, 61-65	328.38	11	60	8	16
36X-2, 33-39	329.63	11	48	20	21
36X-5, 92-98	334.12	13	46	15	25
37X-2, 33-40	339.73	<5	74	10	12
37X-3, 66-68	341.52	<5	61	23	15
37X-5, 92-100	344.81	6	45	26	20
38X-2, 33-35	348.93	9	60	13	18
38X-5, 92-94	355.02	12	61	14	14
39X-2, 33-38	359.53	6	54	17	20
39X-4, 35-37	362.55	12	62	14	12

Table 3 (continued).

Core, section, interval (cm)	Depth (mbsf)	Smectites (%)	Illite (%)	Kaolinite (%)	Chlorite (%)
39X-5, 90-95	364.60	7	71	10	12
39X-CC, 17-19	364.82	10	52	13	14
40X-1, 43-45	367.83	11	63	16	10
40X-CC, 33-35	368.23	<5	65	16	16
41X-CC, 21-23	377.21	9	65	13	13
42X-CC, 25-27	386.85	9	63	12	16
42X-CC, 28-30	386.88	8	62	12	18
44X-1, 103-105	406.93	6	64	13	17
44X-2, 33-38	407.73	13	67	8	12
44X-2, 52-54	407.92	9	77	8	6
44X-CC, 10-12	408.12	10	71	10	9
47X-2, 21-23	436.51	11	69	10	10
47X-2, 29-31	436.59	13	63	12	13
47X-2, 38-40	436.68	13	64	10	14
47X-2, 41-45	436.71	9	71	7	13
47X-3, 145-147	439.25	6	70	15	10
47X-4, 02-04	439.32	14	59	11	16
47X-4, 73-75	440.03	7	76	7	10
47X-4, 76-78	440.06	16	64	8	12
47X-CC, 02-04	440.17	8	74	6	12
47X-CC, 05-08	440.20	13	62	8	17
48X-1, 23-25	444.73	14	62	14	10
48X-1, 60-62	445.10	10	75	6	10
48X-1, 64-66	445.14	9	63	10	18
48X-2, 9-11	446.09	13	64	12	11
48X-2, 33-35	446.33	12	66	5	10
48X-2, 40-42	446.40	7	70	10	10
51X-1, 66-68	473.96	19	55	15	11
51X-1, 72-74	474.02	14	59	13	14
51X-1, 83-85	474.13	8	64	14	14
52X-1, 9-11	482.89	10	70	6	14
52X-1, 28-30	483.08	6	65	10	17
52X-1, 42-44	483.22	7	65	11	18
53X-1, 09-11	492.49	7	75	7	12
53X-1, 15-17	492.55	7	75	9	7
53X-1, 76-78	493.16	8	64	18	11
53X-1, 92-94	493.32	13	60	17	10
53X-2, 6-8	493.96	9	57	10	18
53X-CC, 18-20	494.37	12	61	10	16
54X-1, 27-29	502.27	5	70	10	15
54X-1, 45-47	502.45	10	55	17	18
56X-1, 47-49	518.77	<5	52	20	24
56X-3, 72-74	521.25	11	55	12	21
56X-4, 47-49	522.50	5	62	13	20
56X-5, 108-110	524.61	<5	66	15	16
56X-7, 113-115	526.02	7	44	24	25
57X-1, 92-94	526.22	7	58	17	18
57X-3, 143-145	529.73	8	52	20	20
57X-4, 45-47	530.25	8	60	13	17
58X-1, 45-47	535.35	11	56	16	16
58X-1, 51-53	535.41	15	57	14	14
58X-3, 92-94	537.88	6	71	12	10
58X-5, 79-81	540.74	23	45	18	13
58X-8, 47-49	544.37	22	39	15	24
59X-2, 2-4	546.12	12	53	23	12
59X-2, 8-10	546.18	14	52	17	17
59X-4, 66-70	549.76	18	55	12	15
60X-4, 52-55	558.12	14	52	17	17
60X-6, 120-123	561.72	10	51	26	15
60X-8, 37-40	563.87	13	62	15	21
61X-4, 66-75	567.93	13	47	25	14
61X-6, 125-123	571.52	20	47	15	9
61X-7, 23-25	571.87	17	56	17	10
61X-8, 8-10	573.22	56	23	8	13
61X-CC, 17-19	573.82	39	39	14	8
62X-CC, 5-8	573.55	63	21	8	8
63X-1, 50-54	583.60	82	14	<5	<5
63X-2, 74-79	585.34	79	16	<5	<5
63X-3, 56-59	586.66	64	30	<5	<5
63X-4, 40-42	588.00	68	26	<5	<5
63X-4, 68-71	588.28	81	14	<5	<5
63X-4, 76-78	588.36	76	19	<5	<5
63X-6, 123-126	591.83	79	12	6	<5
63X-7, 32-36	592.42	74	19	<5	<5
64X-1, 32-34	593.12	60	26	9	<5
64X-2, 119-121	595.49	40	39	12	8
64X-3, 22-24	596.02	50	22	18	10
64X-4, 56-58	597.86	44	37	12	6
64X-6, 43-45	600.73	51	33	11	6
64X-CC, 18-20	602.48	48	24	13	7
65X-2, 145-147	605.15	32	38	20	10
66X-3, 59-61	614.39	39	35	18	8
66X-5, 56-58	617.16	26	46	20	8
66X-8, 43-46	621.43	34	44	14	8
70X-6, 30-32	648.70	25	28	27	20
70X-7, 16-18	649.26	33	37	20	10
71X-1, 87-89	651.37	27	46	20	7
71X-2, 15-17	651.15	59	24	12	5
71X-3, 14-16	653.14	53	27	14	6

Table 4. Hole 977A clay mineral abundance from X-ray diffraction data.

Core, section, interval (cm)	Depth (mbsf)	Smectites (%)	Illite (%)	Kaolinite (%)	Chlorite (%)
161-977A-					
1H-1, 29-34	0.32	15	63	8	14
2H-2, 83-88	6.33	26	52	8	14
2H-5, 79-84	11.20	<5	66	10	16
3H-5, 82-84	20.32	<5	71	10	15
4H-1, 70-72	23.70	27	50	10	13
4H-5, 80-82	29.80	<5	70	12	16
5H-2, 80-82	34.80	<5	72	13	13
6H-2, 80-84	44.30	14	64	11	11
7H-1, 72-74	61.80	43	39	9	9
7H-2, 6-11	53.02	9	61	12	19
8H-4, 149-150	66.99	19	51	12	17
8H-6, 12-14	68.62	15	62	11	13
9H-3, 83-87	74.33	14	67	9	10
9H-5, 75-77	77.25	38	34	12	15
10H-1, 88-89	80.88	14	64	8	13
10H-1, 90-91	80.90	18	58	12	12
10H-7, 69-71	89.69	<5	70	10	17
10-CC, 4-6	89.80	11	72	7	10
11H-2, 117-119	92.17	6	73	8	13
11H-3, 16-19	93.13	13	61	12	13
11H-3, 24-26	92.74	8	59	15	18
11H-3, 44-46	92.94	9	63	14	14
11H-3, 49-51	92.99	18	70	8	5
11H-3, 58-59	93.08	26	64	5	5
11H-4, 106-108	93.84	16	52	15	17
12H-3, 25-27	102.25	34	51	7	8
12H-3, 59-61	102.59	22	61	7	10
12H-3, 86-88	102.86	15	63	8	14
12H-4, 39-41	103.89	28	42	10	20
12H-4, 60-62	104.10	5	63	17	15
12H-5, 125-127	106.25	6	73	10	10
13H-1, 30-32	108.80	7	71	10	12
13H-3, 27-29	111.77	18	57	12	14
13H-3, 101-103	112.51	8	60	15	17
13H-4, 57-59	113.57	20	61	7	12
13H-3, 126-128	113.70	10	69	8	13
13H-5, 11-13	114.61	<5	66	12	20
14H-1, 14-16	118.14	16	66	8	10
14H-4, 92-94	123.42	10	70	10	14
14H-5, 136-138	125.36	10	66	12	12
14H-6, 12-14	125.68	13	64	10	13
15H-5, 6-8	133.56	12	64	10	14
17H-5, 100-102	153.50	6	69	12	13
17H-6, 27-29	154.27	10	66	12	12
18X-5, 102-104	163.02	9	72	9	10
19X-4, 26-28	170.36	14	58	14	14
21X-7, 19-21	194.09	13	64	8	14
23X-6, 47-49	211.97	17	57	10	16
24X-3, 79-84	217.39	18	51	12	18
24X-4, 60-98	218.70	10	59	12	19
24X-4, 75-77	218.85	10	62	12	16
25X-3, 80-82	227.03	6	55	19	20
27X-6, 108-110	251.18	16	62	8	13
30X-6, 4-6	278.94	5	68	10	16
31X-1, 127-129	282.27	19	60	9	12
40X-2, 52-56	369.52	<5	68	10	18
41X-6, 3-8	384.63	21	52	10	17

In Unit III at Hole 976B, a consistent decrease in Sr is observed from bottom to top. The most significant fluctuations were found in Unit II (upper Pliocene), where the decrease in these elements is probably a consequence of the high proportion of quartz in these samples. In Unit I (Fig. 5), only slight fluctuations are observed through the whole unit.

At Hole 977A, from which only scattered samples were analyzed, trace elements display trends in Sr, Ba, REEs, and Rb (Fig. 6). Two different intervals can be recognized on the basis of these elements. One interval, from 0 to 61.8 mbsf, has a higher Sr content but lower Ba, REEs, and Rb contents; the other interval, from 61.8 to 379.5 mbsf, has a lower Sr content but higher Ba, REEs, and Rb contents. Sr decreases from the lower interval upward, whereas Ba, REEs, and Rb increase. Cu shows no particular trend in this hole, but has an isolated positive anomaly.

DISCUSSION

Sedimentary Facies

The sedimentary facies at Sites 976 and 977 are dominated by hemipelagites and fine-grained turbidites, and less common homogeneous gravity flows, contourites, and debris flows. These sedimentary facies resulted from pelagic settling of terrigenous particles and marine microskeletons, turbidite currents, low density gravity flows, bottom currents, and debris flows (Alonso et al., Chap. 4, this volume; Shipboard Scientific Party 1996a, 1996b). In the West Alboran Basin (Site 976), submarine canyons governed the terrigenous input into the basin. Four submarine canyons indent the slope of the northwestern Alboran Sea (Ercilla et al., 1992); the sediment supply from one of those canyons—the Fuenguirola canyon—was the main pathway for terrigenous material during the Pliocene and Pleistocene in this area. Three different sedimentary stages have been invoked to explain the depositional history at Site 976. Stage I (early Pliocene) is characterized by hemipelagic settling and low-energy turbidite currents; during Stage II (early Pleistocene/late Pliocene), resedimented facies (turbidite currents, bottom currents, and debris flows) developed; and during Stage III (Pleistocene), hemipelagic settling and low-energy gravity flows dominated (Alonso et al., Chap. 4, this volume).

Changes in facies also correspond to different sedimentation rates over time (Fig. 8). At Site 976, the average sedimentation rates were 15 m/m.y. for the upper Miocene, 453 m/m.y. for the early Pliocene, 340 m/m.y. for the late Pliocene, and 208 m/m.y. for the Pleistocene (Shipboard Scientific Party, 1996a). Average sedimentation rates at Site 977 were 96 m/m.y. for the late Pliocene–late early Pliocene and 154 m/m.y for the Pleistocene (Shipboard Scientific Party, 1996b). Different types of facies at Site 976 can also be correlated with different mineral abundances. Hemipelagites are richer in calcite (20%–50%) and clays (35%–60%), with a lower content of quartz (15%–20%) and dolomite (<5%–10%). In turbidite facies, the Td to Ta intervals are richer in quartz (30%–60%), but have lower amounts of dolomite (5%–35%), clays (10%–30%), and calcite (15%–25%), whereas the Te interval is richer in clay (40%–60%), with lower amounts of calcite (20%–45%), quartz (25%–30%), and dolomite (<5%). Gravity-flow facies are richer in clays (30%–50%) and quartz (15%–25%), contourites are richer in clays (20%–40%), quartz (15%–25%), and dolomite (<5%–55%), and debris-flow facies are richer in quartz (25%–40%) and dolomite (20%–60%; see also Alonso et al., Chap. 4, this volume).

The influx of terrigenous components is clearly reflected by the higher silt to sand fraction, mainly represented by quartz, feldspar, detrital dolomite, and rock fragments resulting from erosion of the emerged areas. Turbidite, gravity-flow, contourite, and debris-flow facies are also correlated with higher sedimentation rates (Fig. 8) during the early/late Pliocene (Unit II in Hole 976B). In hemipelagic facies, the two different types of hemipelagites (Alonso et al., Chap. 4, this volume) correspond to a higher clay content (35%–60%) with a lower calcite content (15%–30%), and to a lower clay content (35%–50%) with a higher calcite content (25%–50%; Pl. 1, figs. 2, 3). Periods of high and low carbonate production are an important factor controlling variations in terrigenous vs. calcite content; however, variations in the terrigenous input in the Alboran basin have played an important role as well, and it is difficult to distinguish between the effect of dilution by terrestrial clastic and carbonate production without other proxies to evaluate changes in calcareous biogenic productivity in hemipelagites.

Mineral Provenance

The two main sources of sediment supply in the Alboran Basin are biogenic and terrigenous. Except for siliceous organisms, which occur in scattered intervals within the studied sediments, the biogenic input is mainly represented by calcite. Foraminifers and nannofossils are the main source of this mineral. As mentioned above, carbonate production and terrigenous input control calcite fluctuations, and no evidence of dissolution was observed in the sediments. The lower calcite content in fine-grained resedimented facies can be explained by a dilution of the biogenic content by detrital components. In hemipelagites, calcite fluctuations can record both variations in terrige-

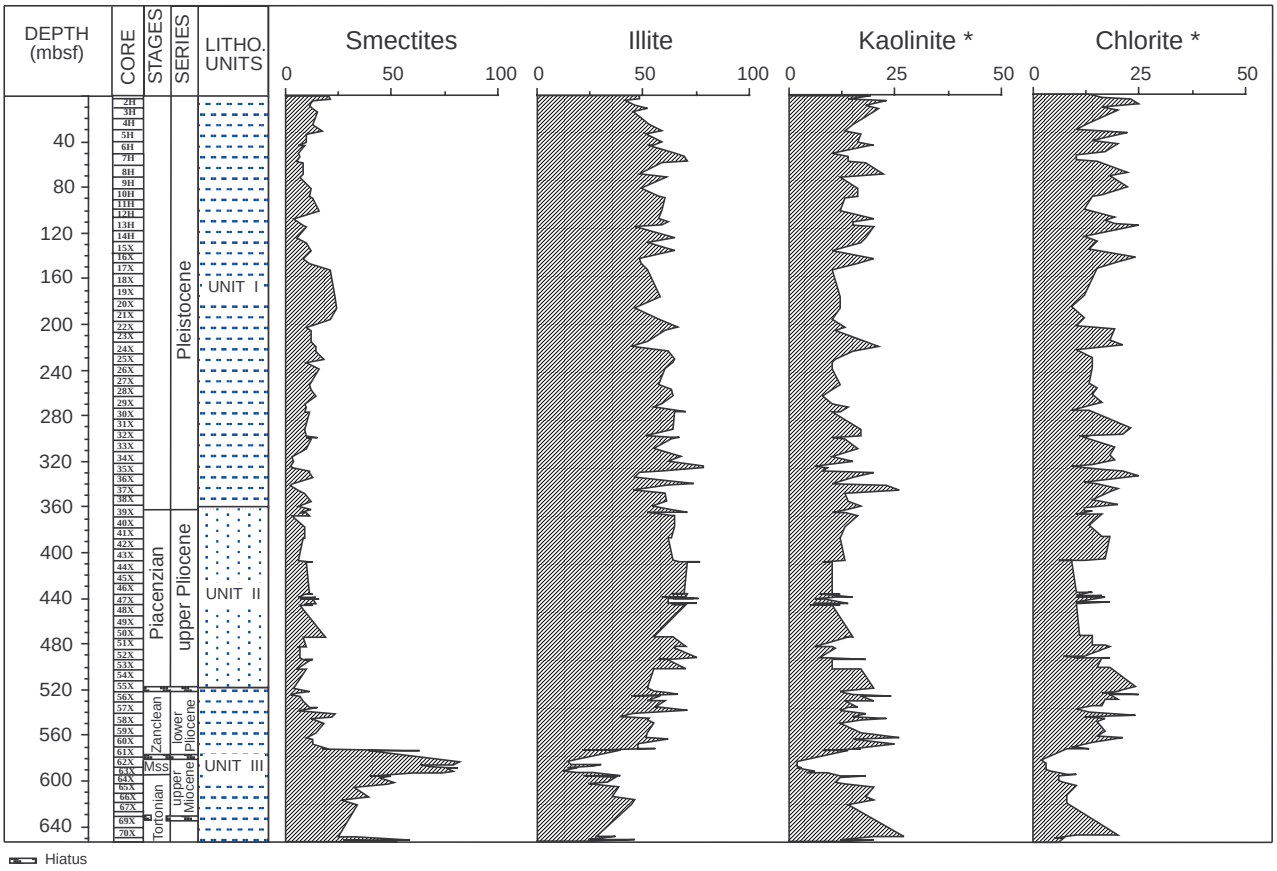

Figure 4. Clay mineralogy, Hole 976B.

nous accumulation or variations in paleoproductivity. One of the classic tracers of paleoproductivity, Ba (e.g., Bishop, 1988), was analyzed in only a few samples in this study, and no conclusive results were obtained for changes in paleoproductivity controlling biogenic content. In work in progress, we hope to determine whether calcite content could be correlated with other proxies for paleoproductivity, especially during deposition of ORLs. Preliminary results indicate that the Ba content is very low, thus indicating no enhanced productivity periods. Furthermore, in most of the samples, Ba appears to behave similarly to detrital elements such as Rb or REEs. Only in the uppermost Pleistocene deposits can higher Ba content (Fig. 7) be correlated with higher calcite content (Fig. 3) at Site 977, and only one isolated positive anomaly is observed in coeval sediments at Site 976 (Fig. 6). Higher resolution sampling and barite content analyses, which are a better indicators than Ba for paleoproductivity (Paytan, 1995), are needed. Sr content in these sediments (Figs. 6, 7) appears to be related to calcite.

Feldspar proportions are relatively low and form silt- to sand-sized grains. Quartz is more abundant in resedimented facies and different morphologies are observed in these sediments, from rounded to angular grains (Pl. 1, figs. 3, 4). The coexistence of quartz grains with rounded and angular morphologies suggests the possible contribution of emerged older sedimentary rocks and recycling of previously detrital quartz into the basin. Lithic fragments are mainly from metamorphic rocks and indicate nearby provenance.

Dolomite is especially abundant (up to 60%) in some resedimented facies from the upper Pliocene deposits from Hole 976B (Unit II). The two types of dolomite observed in these sediments support different origins for this mineral. Detrital dolomite grains (Pl. 1, fig. 5) are thought to proceed from erosion of the emerged areas in the Iberian margin, either from metamorphic dolomite from the Alpujarride Complexes (Betic Cordilleras) or from Messinian dolomite cropping out on land. Diagenesis of these levels rich in detrital dolomite led to the neoformation of smaller dolomite crystals with euhedral morphology (Pl. 1, fig. 6). Circulation of fluids becoming enriched in Mg at these (probably) higher primary-porosity levels could have contributed to additional dolomitization of any primary calcite content, which may explain the notable depletion in calcite (<5%) in some intervals (Fig. 2).

Concerning the clay mineral assemblages, the existence of similar components in all types of facies suggests a common source area. However, climatic, tectonic, and eustatic factors controlling the source rocks, routes of sediment supply, and sediment transport pathways have resulted in differences in the abundance of clay minerals in these assemblages.

Detrital mica is a common terrigenous component resistant to degradation during transport, and usually represents the contribution of an unaltered source rock, as results from physical weathering in the source areas (e.g., Velde, 1985; Chamley, 1989). Composition, sizes, and morphologies of the illites in the studied sediments support a detrital origin, and they can therefore be considered as detrital micas. During transport and deposition, only micas of smaller grain size could have been degraded. However, degradation is not very important, and micas from the silt or even sand fraction are very well preserved (Pl. 1, fig. 5), which provides evidence for an origin by physical weathering of the emerged metamorphic rocks. The presence of smectite and I/S mixed-layers also precludes a possible diagenetic origin for the illite. The chemical compositions indicate trends typical of most of the muscovites from the Betic Cordilleras (Martin-Ramos, 1976; Nieto et al., 1989). The increase in mica content may be related to rejuvenation of subaerial reliefs by a sea-level fall or by tectonic uplift and to the relative importance of physical weathering (Chamley, 1989). At Site 976, the higher illite content in the upper Pliocene sediments (Unit II) can be correlated with the fall in sea level at this time, which is also recorded by a change in sedimentary facies and higher sedimentation rates (Fig. 8).

Table 5. Normalized formula for smectites from Hole 976B.

Depth (mbsf)	Si	^{IV}Al	^{VI}Al	Mg	Fe	Ti	Σ_{oct}	K	Ca	Σ_{int}
24.80	3.75	0.25	1.18	0.30	0.55	—	2.03	0.19	0.13	0.32
	3.73	0.27	1.35	0.27	0.45	0.01	2.08	0.35	0.01	0.36
	3.86	0.14	1.60	0.17	0.25	0.01	2.03	0.30	—	0.30
	3.79	0.21	1.68	0.19	0.18	—	2.05	0.02	—	0.02
	3.73	0.27	1.89	0.11	0.05	—	2.05	0.31	—	0.31
62.30	3.52	0.48	1.74	0.27	0.29	—	2.30	0.18	—	0.18
128.80	3.95	0.05	1.56	0.14	0.32	0.01	2.03	0.06	—	0.18
339.73	3.62	0.48	1.31	0.34	0.34	—	1.99	0.24	—	0.24
	3.65	0.35	1.86	0.15	0.15	—	2.16	0.15	—	0.15
	3.79	0.21	1.55	0.28	0.25	—	2.08			
	3.84	0.16	1.55	0.14	0.28	0.04	2.01	0.14	0.02	0.16
	3.72	0.23	1.77	0.18	0.12	—	2.07	0.26	—	0.26
367.83	3.86	0.14	1.29	0.39	0.36	—	2.04	0.31	0.06	0.37
	3.73	0.27	1.62	0.17	0.20	0.02	2.01	0.33	—	0.33
	3.78	0.22	1.35	0.32	0.44	—	2.11	0.28	—	0.28
408.12	3.58	0.42	1.60	0.32	0.30	—	2.22	0.18	0.02	0.20
436.63	3.77	0.23	1.38	0.36	0.33	—	2.07	0.35	0.06	0.41
	3.87	0.13	1.32	0.57	0.20	—	2.09	0.35	—	0.35
439.32	3.59	0.41	1.12	0.48	0.48	0.02	2.10	0.32	—	0.32
	3.83	0.17	1.22	0.40	0.51	—	2.13	0.18	0.04	0.22
502.45	3.49	0.51	1.41	0.45	0.34	0.03	2.23	0.27	0.01	0.28
	3.87	0.13	1.43	0.35	0.24	0.04	2.06	0.27	—	0.27
571.87	3.52	0.48	1.69	0.25	0.26	—	2.20	0.09	—	0.09
	3.85	0.15	1.51	0.29	0.29	0.01	2.10	0.12	0.03	0.15
	3.85	0.15	1.53	0.28	0.27	—	2.08	0.22	0.02	0.24
573.82	3.86	0.14	1.56	0.35	0.20	0.01	2.12	0.10	—	0.10
	3.81	0.18	1.49	0.32	0.28	—	2.09	0.20	0.02	0.22
	3.88	0.12	1.78	0.16	0.10	—	2.04	0.36	—	0.36
	3.77	0.23	1.43	0.44	0.23	—	2.10	0.29	0.03	0.32
	3.85	0.15	1.65	0.16	0.19	—	2.00	0.29	—	0.29
	3.74	0.26	1.35	0.45	0.25	0.03	2.08	0.35	0.04	0.39
573.90	3.90	0.10	1.40	0.41	0.26	—	2.07	0.25	—	0.25
	3.68	0.32	1.43	0.36	0.37	0.01	2.17	0.27	0.02	0.29
	3.87	0.13	1.45	0.49	0.25	—	2.19	0.05	0.02	0.07
588.36	3.75	0.25	1.39	0.28	0.31	0.06	2.04	0.23	0.05	0.28
	3.68	0.32	1.55	0.33	0.24	0.01	2.13	0.22	0.03	0.25
599.23	3.80	0.20	1.18	0.49	0.48	0.02	2.17	0.08	0.04	0.12
	3.85	0.15	1.28	0.30	0.48	—	2.06	0.20	0.03	0.23
	3.68	0.32	1.55	0.33	0.24	0.01	2.13	0.22	0.03	0.25
642.71	3.93	0.07	1.43	0.32	0.32	0.00	2.07	0.26	0.01	0.27
	3.76	0.24	1.28	0.32	0.50	0.01	2.11	0.17	0.03	0.20
	3.77	0.23	1.86	0.07	0.12	0.01	2.06	0.02	0.03	0.05
	3.91	0.09	1.27	0.32	0.38	0.01	1.98	0.23	0.16	0.39

Notes: — = 0.00. Σ_{oct} = sum of octahedral cations; Σ_{int} = sum of interlayer cations.

In the studied samples, chlorite is mostly of detrital origin. This mineral is not resistant to transport and weathering, which indicates proximal source areas and a relatively important physical weathering. Chlorite in the studied samples shows a wide range of basal spacing, pointing to a provenance from both the Nevado-Filabride and Alpujarride Complexes (Nieto, 1983, 1997). Kaolinite, in contrast, is resistant to transport and mainly forms in hydrolyzing conditions because of chemical weathering (Singer, 1980; Maillot and Robert, 1980; Chamley, 1989). Kaolinite fluctuations in the studied sediments can be interpreted as the results of fluctuations in the detrital supply and as consequences of climatic changes that favored the formation of kaolinite in the source areas.

Smectites can originate from diagenetic processes (Brosse, 1982), neoformation in a Mg-rich environment (Weaver and Beck, 1977), alteration of volcanic rocks (Fisher, 1977), or in soils under hydrolyzing conditions (Thirty, 1981; Chamley, 1989). The chemical composition of smectites varies according to the genetic environment. Al-Fe beidellite, of particular interest here, results from reworking of soils. The chemical compositions of the smectites from these sediments indicate a detrital origin and a provenance from soils in the source areas. A high content of detrital Al-Fe beidellite implies chemical weathering, and, therefore, fluctuations in smectite content in the samples can be related to climate changes (Chamley, 1989). Increasing smectite through the middle Pleistocene indicate warming climate conditions. The four intervals we noted in the upper Pleistocene sediments for higher/lower smectite content (Fig. 4) could be related to the alternation of cooler and warmer climatic periods. Further and higher resolution studies of smectite content at both sites may allow a better correlation of the Alboran site sequences with climate cycles in the western Mediterranean. The increase in smectites and kaolinite along with the decrease in illite by the latest Pleistocene is probably related to climate warming and also to an increase in coeval tectonic stability.

A significant change in smectite abundance (up to 80%) is observed in the Messinian deposits. The Messinian deposits, as in other Mediterranean areas (Chamley, 1989), represent a noticeable break in the clay mineralogy. Smectite contents increase sharply in comparison with the Tortonian and Pliocene deposits, and their smectite composition (Fe-Al beidellite type) indicates development in soils, most likely in a subarid climate. The smectites probably formed from the erosion and reworking of soils that likely developed during the Messinian. Development of smectite in the peri-Mediterranean soils could have been favored by the alternation of dry and wet episodes (Chamley and Robert, 1980). These mineralogical changes seem to be restricted to the Messinian period as a consequence of the relative aridification of the Mediterranean borderlands.

Table 6. Normalized formula for smectites from Hole 976B.

Depth (mbsf)	Si	^{IV}Al	^{VI}Al	Mg	Fe	Ti	Σ_{oct}	K	Ca	Σ_{int}
0.32	3.50	0.50	1.68	0.23	0.29	—	2.20	0.15	0.02	0.17
	3.44	0.66	1.34	0.32	0.34	—	2.00	0.27	—	0.27
92.00	3.65	0.35	1.49	0.50	0.21	—	2.20	0.34	—	0.34
	3.42	0.58	1.79	0.35	0.15	—	2.29	0.32	0.01	0.33
	3.28	0.72	0.75	1.42	0.44	—	2.61	0.28	—	0.28
	3.51	0.42	1.78	0.20	0.20	—	2.18	0.24	—	0.24
108.00	3.54	0.46	1.66	0.32	0.32	—	2.30	0.27	0.01	0.28
164.86	3.72	0.28	1.22	0.48	0.35	—	2.05	0.27	0.09	0.36
	3.61	0.39	1.40	0.41	0.37	—	2.18	0.25	0.02	0.27
	3.79	0.21	1.63	0.36	0.31	—	2.30	0.05	0.03	0.08
264.72	3.61	0.39	1.65	0.33	0.32	—	2.30	0.25	0.01	0.26
	3.60	0.40	1.48	0.55	0.40	0.01	2.43	0.30	—	0.30
	3.85	0.15	1.54	0.35	0.33	—	2.22	0.13	0.01	0.14
333.93	3.66	0.44	1.25	0.39	0.40	—	2.04	0.21	0.04	0.25
	3.40	0.60	1.43	0.34	0.24	—	2.01	0.22	—	0.22
	3.73	0.27	1.38	0.43	0.33	—	2.14	0.27	—	0.27
389.07	3.73	0.27	1.82	0.13	0.13	—	2.08	0.14	0.02	0.16
	3.90	0.10	1.18	0.57	0.35	—	2.10	0.24	0.09	0.33
	3.54	0.46	1.69	0.32	0.26	—	2.27	0.30	0.02	0.32
453.59	3.64	0.36	1.54	0.23	0.27	0.01	2.04	0.16	0.02	0.18
	3.65	0.35	1.50	0.33	0.29	0.02	2.12	0.14	0.06	0.20
	3.65	0.35	1.38	0.33	0.33	—	2.04	0.38	0.12	0.50
	3.84	0.16	1.34	0.56	0.25	—	2.15	0.22	—	0.22
488.39	3.71	0.29	1.64	0.27	0.22	—	2.13	0.13	0.02	0.15
	3.76	0.24	1.66	0.16	0.23	—	2.05	0.14	0.06	0.20
521.66	3.63	0.37	1.14	0.21	0.71	—	2.06	0.32	0.07	0.39
	3.71	0.29	1.51	0.25	0.32	—	2.08	0.16	0.10	0.26

Notes: — = 0.00. Σ_{oct} = sum of octahedral cations; Σ_{int} = sum of interlayer cations.

Table 7. Normalized formula for illite/smectite (I/S) mixed layers for Holes 976B and 977A.

Depth (mbsf)	Si	^{IV}Al	^{VI}Al	Mg	Fe	Ti	Σ_{oct}	K	Ca	Σ_{int}
161-976A-										
24.80	3.39	0.61	0.72	0.62	0.85	0.09	2.28	0.44	—	0.44
62.30	3.41	0.59	1.54	0.29	0.31	0.00	2.14	0.53	0.02	0.55
62.30	3.37	0.63	1.84	0.23	0.12	0.00	2.19	0.63	—	0.63
128.80	3.52	0.48	1.74	0.19	0.14	0.04	2.11	0.43	—	0.43
408.12	3.27	0.73	1.99	0.15	0.08	0.00	2.22	0.60	—	0.60
408.12	3.62	0.48	1.59	0.38	0.15	0.00	2.12	0.51	—	0.51
571.87	3.40	0.60	1.76	0.25	0.10	0.00	2.11	0.60	—	0.60
588.36	3.52	0.48	1.49	0.29	0.33	0.00	2.11	0.53	—	0.53
599.23	3.50	0.50	1.62	0.29	0.19	0.00	2.10	0.48	—	0.48
642.71	3.46	0.54	1.88	0.11	0.08	0.03	2.10	0.44	—	0.44
642.71	3.52	0.48	1.67	0.30	0.13	0.00	2.10	0.46	—	0.46
642.71	3.43	0.57	1.77	0.13	0.10	0.03	2.03	0.54	—	0.54
161-977A-										
0.32	3.43	0.57	1.39	0.30	0.54	—	2.23	0.54	0.01	0.55
	3.78	0.22	0.86	0.55	0.69	—	2.10	0.59	0.02	0.61
	3.23	0.77	1.89	0.17	0.14	—	2.20	0.68	—	0.68
	3.40	0.60	1.68	0.35	0.24	—	2.27	0.44	0.01	0.45
108.00	3.57	0.43	1.43	0.42	0.37	0.01	2.22	0.43	0.04	0.47
	3.25	0.75	1.94	0.18	0.06	—	2.18	0.53	—	0.53
164.86	3.56	0.44	1.02	0.64	0.59	—	2.25	0.40	0.01	0.41
264.72	3.67	0.33	1.35	0.49	0.41	—	2.25	0.40	0.07	0.47
	3.43	0.57	1.59	0.13	0.20	—	1.92	0.64	—	0.64
333.93	3.31	0.69	1.83	0.19	0.11	—	2.13	0.65	—	0.65
	3.65	0.35	1.39	0.39	0.37	—	2.15	0.41	—	0.41
389.07	3.66	0.44	1.17	0.49	0.36	—	2.02	0.54	0.08	0.62
	3.54	0.46	1.69	0.32	0.26	—	2.27	0.30	0.02	0.32
453.59	3.65	0.35	1.38	0.33	0.33	—	2.04	0.38	0.12	0.50
488.39	3.44	0.56	1.84	0.27	0.09	—	2.20	0.57	0.09	0.66
521.66	3.55	0.45	1.50	0.31	0.24	—	2.05	0.51	0.04	0.55

Notes: — = 0.00. Σ_{oct} = sum of octahedral cations; Σ_{int} = sum of interlayer cations.

Other clay minerals reported in minor proportions in the studied sediments, such as I/S mixed layers, palygorskite, and sepiolite, are considered to be mainly of detrital origin. I/S mixed layers commonly originate in soils (Chamley et al., 1978; Chamley, 1989) or during diagenetic processes (Pollastro, 1985), but no diagenetic trends were observed at the studied sites, which allows a diagenetic origin to be ruled out. Fibrous clays (palygorskite and sepiolite) may derive from neoformation (chemical precipitation) in some restricted evaporative basins, especially during the Messinian, or from calcareous pedogenic crust, as reported in comparable marine realms (Chamley, 1989). These minerals can be easily reworked by wind or water and, in these sediments, can be considered to be of detrital origin. This fact is supported by the scattered presence of isolated fibers in most of the samples. However, the circulation of Mg-rich fluids and Mg fixation

could have given rise to the authigenic fibrous clays in some of the levels.

The emerged areas of Iberia are thought to be the main source of the terrigenous material in the northern West Alboran Basin, whereas in the East Alboran Basin, the African and Iberian margins are both possible sources. Paleozoic to Triassic metamorphic rocks from the metamorphic complexes of the Alboran Domain, older sedimentary rocks, and minor volcanic and ultramafic rocks cropping out in the Betic and Rif Chains were the main sources of the terrigenous fraction (feldspar, quartz, rock fragments, detrital dolomite, and clays) in the samples. Eolian input can also be considered a minor source of detrital components over time.

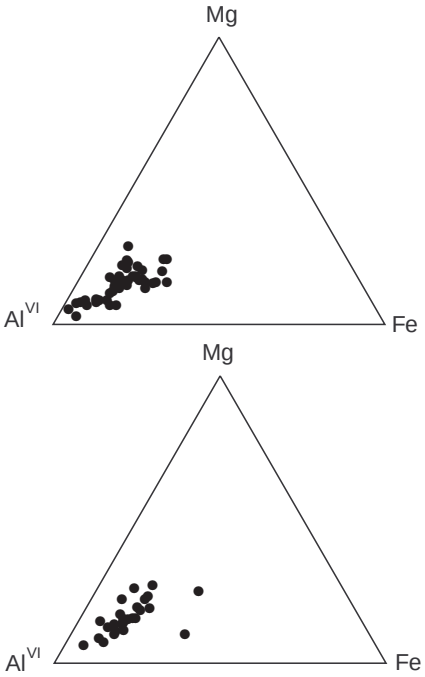

Figure 5. Al-Fe-Mg diagrams (Weaver and Pollard, 1973) showing smectite composition at Holes 976B **(top)** and 977A **(bottom).**

CONCLUSIONS

Mineral components in the upper Miocene to Pleistocene sequences from the Alboran Basin indicate that these sediments mainly formed from biogenic input and terrigenous supply, with a minor contribution of neoformed phases. Detrital components are mainly quartz, feldspar, rock fragments, detrital dolomite, and clays. No diagenetic influence linked to depth of burial has been observed that could obliterate the primary signal of deposition; thus, terrigenous components reflect primary sedimentary signals and provide information on sedimentary processes and source areas. In the upper Miocene deposits, no significant trends in bulk mineral components were observed, except some fluctuations in calcite vs. clay mineral content. However, the Messinian deposits represent a noticeable break in clay mineral abundance with a significant increase in smectites. Smectite composition indicates that they correspond to Al-beidellites that probably were derived from the erosion and reworking of soils that developed during the Messinian. Soil development could have been favored by the alternation of dry and wet episodes and the relative aridification of the Mediterranean borderlands. Bulk mineral fluctuations in lower Pliocene samples correspond to variations in calcite vs. clay content, and no major trends were observed in detrital components or detrital trace elements, although differences in clay mineral abundances suggest a change in the source area conditions. The increase in kaolinite in upper Pliocene deposits suggests the rel-

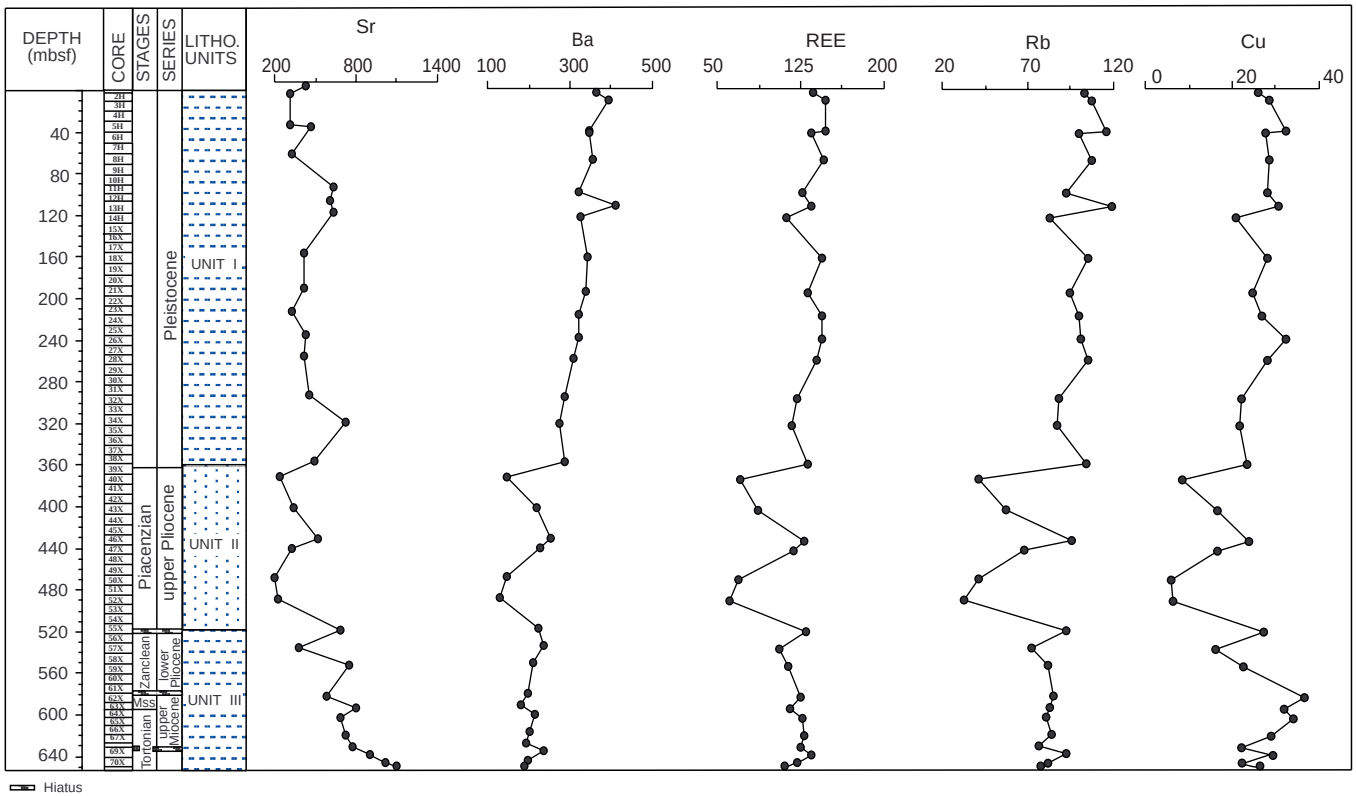

Figure 6. Geochemical trends at Hole 976B.

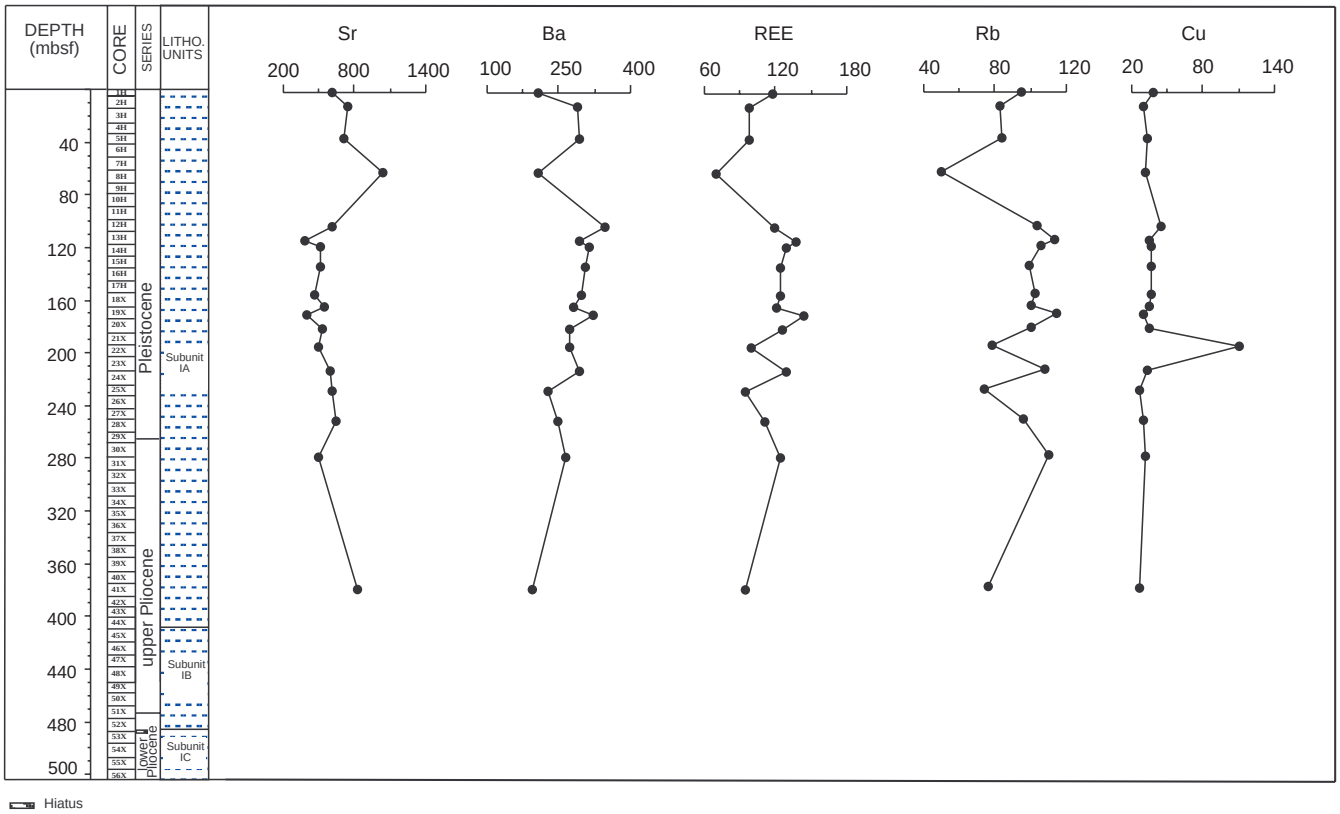

Figure 7. Geochemical trends at Hole 976B.

Table 8. Geochemical data, Hole 976B.

Depth (mbsf)	Sr (ppm)	Ba (ppm)	Rb (ppm)	REE (ppm)	Zr (ppm)	V (ppm)	Ni (ppm)	Cu (ppm)	Zn (ppm)	Co (ppm)	Pb (ppm)	U (ppm)	Th (ppm)
3.48	424	363	103	136.70	90.7	113.34	58.63	26.06	98.26	11.96	14.39	2.38	7.70
11.06	318	394	107	147.90	106.5	119.19	46.78	28.61	106.65	12.20	16.88	2.98	8.66
40.40	316	345	116	147.77	93.41	23.10	66.22	32.43	117.19	15.16	18.08	3.07	8.50
43.31	465	345	100	135.14	82.91	12.04	47.27	27.66	96.61	12.66	15.44	3.02	7.72
68.90	323	356	108	145.24	100.51	18.30	45.38	28.42	96.49	11.57	15.64	2.46	8.29
100.30	636	322	93	126.56	77.61	10.67	73.16	28.13	86.98	14.02	14.73	2.85	7.29
113.44	607	412	119	134.71	87.2	94.17	51.02	30.75	89.14	10.07	13.22	3.54	7.56
124.45	639	324	83	112.35	70.4	92.77	52.43	20.96	96.81	9.88	13.69	2.04	6.32
164.20	412	342	105	144.29	91.4	123.87	51.76	28.13	142.71	12.33	17.11	2.73	8.31
196.20	412	337	94	131.34	98.3	111.11	53.19	24.68	96.79	11.08	13.83	2.65	7.58
220.26	329	322	100	143.63	93.2	126.36	48.45	26.98	97.64	12.78	15.54	2.47	8.15
241.31	429	323	101	144.30	84.8	156.05	88.27	32.27	94.28	24.28	18.71	3.63	8.29
262.83	412	307	105	140.13	89.3	121.00	66.08	27.89	99.17	13.80	17.68	2.72	8.19
299.09	458	285	88	121.63	68.2	96.62	51.53	22.18	80.42	10.60	17.10	2.46	7.07
325.78	726	274	87	116.57	79.1	100.42	50.63	21.90	34.52	10.70	14.96	2.26	6.89
362.55	497	285	104	131.71	86.6	107.49	63.73	23.29	93.01	12.29	13.35	2.56	7.53
377.05	237	148	42	71.17	26.3	42.67	52.74	8.47	56.55	7.28	7.37	1.14	3.85
407.92	343	219	57	86.03	52.2	97.16	119.29	16.55	67.70	14.61	12.81	1.61	4.84
436.71	519	254	96	127.90	77.0	102.69	56.49	23.83	80.36	14.16	16.69	3.21	7.42
446.09	333	229	68	118.26	51.3	72.13	83.96	16.61	65.90	13.46	11.83	1.99	6.81
473.39	203	147	41	68.72	30.7	43.05	50.78	6.00	42.28	6.84	6.59	1.23	3.70
493.96	229	131	33	60.62	33.4	34.66	50.44	6.57	32.71	7.20	6.56	0.97	3.37
524.61	686	225	92	129.42	82.9	122.79	67.95	27.17	120.88	13.01	15.45	2.11	7.18
540.74	377	235	73	106.50	70.7	67.87	106.66	16.37	90.98	23.03	13.12	1.81	6.14
558.12	746	211	81	114.20	83.3	112.90	56.16	22.44	110.01	10.84	17.85	2.03	6.50
588.28	588	196	85	125.62	85.2	107.48	49.31	36.40	85.95	13.27	18.54	2.82	6.87
597.86	799	181	83	115.88	83.5	100.83	46.56	31.86	78.81	12.11	17.90	2.32	6.50
608.20	684	213	80	126.13	84.6	114.53	39.58	33.96	79.43	11.24	17.73	1.92	6.76
623.90	722	203	84	127.87	94.3	130.01	48.89	29.08	84.67	11.86	22.09	1.89	7.03
635.79	770	193	76	125.54	85.8	120.06	32.87	21.95	77.66	11.08	18.84	2.76	6.59
642.71	904	238	92	135.04	93.7	127.67	45.56	29.15	96.15	15.04	30.07	2.27	7.24
653.14	1013	200	81	121.78	92.5	125.05	35.23	22.38	91.59	10.90	18.71	2.14	6.61
657.92	1121	191	79	110.24	69.1	103.78	36.03	26.52	94.64	11.71	18.77	2.73	5.68

Table 9. Geochemical data, Hole 977A.

Depth (mbsf)	Sr (ppm)	Ba (ppm)	Rb (ppm)	REE (ppm)	Zr (ppm)	V (ppm)	Ni (ppm)	Cu (ppm)	Zn (ppm)	Co (ppm)	Pb (ppm)	U (ppm)	Th (ppm)
0.32	613	208	95	116.91	63.90	106.91	42.75	37.37	91.51	12.41	22.02	2.96	7.65
11.20	743	290	83	97.45	57.75	92.18	56.51	30.27	83.43	12.21	14.73	4.00	6.45
34.50	713	295	84	97.89	56.14	98.26	35.50	32.94	82.39	11.95	14.27	2.36	6.56
61.80	1038	207	50	69.25	34.64	85.10	75.65	32.02	59.72	22.82	11.43	5.48	4.23
102.50	619	348	104	119.61	65.36	110.15	53.53	44.33	96.41	15.64	16.66	2.75	8.23
113.33	385	293	113	137.97	80.87	131.90	59.70	35.19	105.69	16.41	18.65	3.26	9.04
118.14	512	314	106	129.09	72.30	123.21	49.17	36.96	110.40	13.94	16.43	3.07	8.44
133.56	511	305	99	124.16	70.81	104.70	46.31	36.55	91.76	12.72	15.96	3.50	8.21
154.27	465	296	103	124.01	61.05	112.93	52.37	36.26	101.21	14.75	17.40	2.96	8.34
163.02	550	279	100	120.58	70.71	114.15	45.80	35.50	140.32	12.46	19.06	3.11	7.83
170.36	399	322	114	143.60	77.86	138.04	48.46	30.29	101.67	15.99	21.31	2.60	9.57
180.67	523	274	100	125.15	68.39	122.49	65.10	34.82	100.62	18.26	18.39	3.22	8.59
194.09	492	274	78	100.13	47.97	129.04	57.08	111.01	135.72	23.11	15.96	2.32	6.40
211.97	596	295	108	129.03	65.65	121.97	49.42	32.92	216.62	14.28	21.09	2.90	8.61
227.00	604	227	74	94.36	57.43	92.58	40.81	26.08	144.20	10.69	11.61	2.58	6.25
251.18	651	247	95	111.36	46.56	105.17	45.81	30.58	164.36	12.64	17.41	2.54	7.51
278.94	504	265	110	124.40	58.21	119.59	51.89	32.15	126.25	15.18	19.73	2.70	8.40
379.50	830	195	76	94.50	58.60	87.60	39.48	26.73	82.72	12.19	13.30	2.73	6.26

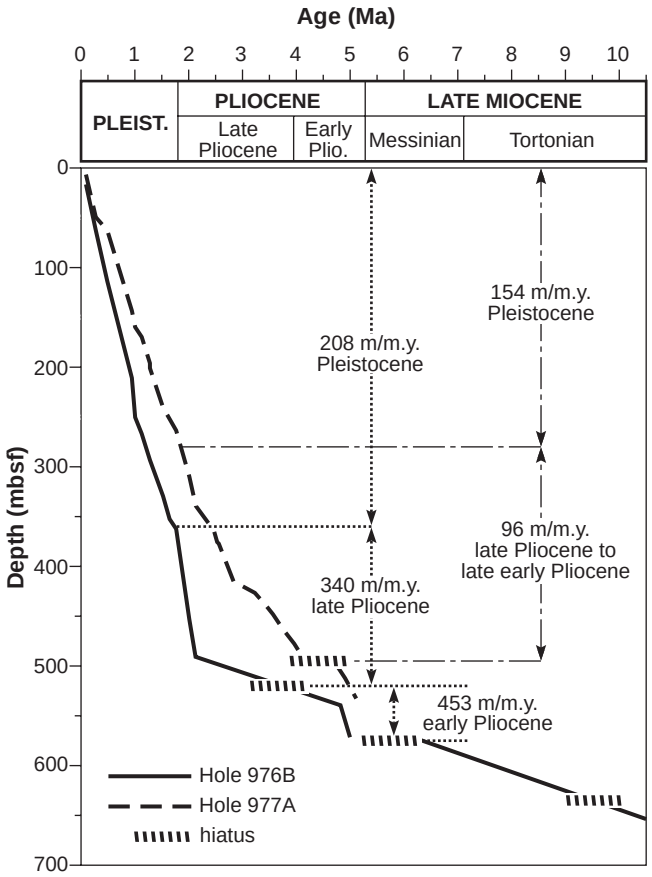

Figure 8. Sedimentation rates at Holes 976B and 977A (data from Shipboard Scientific Party, 1996a, 1996b).

ative importance of chemical weathering; at the same time, the continuous increase in illite at this time also indicates a slight but continuous rejuvenation of subaerial reliefs. However, the composition of these sediments reflects major changes in source areas during the late Pliocene. A notable increase in detrital components is recorded by quartz, detrital dolomite, and detrital mica, and can be correlated to a sea-level fall or to tectonic uplift. The significant increase in dolomite in the uppermost Pliocene deposits could indicate uplifting of dolomite rocks as source of detrital dolomite and therefore increasing tectonic instability during the late Pliocene. Detrital components from Pleistocene samples show no significant variations, and the quartz content is relatively homogeneous through time, except for some turbidite episodes. Fluctuations in clay mineral abundances could reflect not only tectonic factors, but also climate factors controlling source areas. Smectite content variations in upper Pleistocene sediments could be related to the alternation of cooler and warmer climatic periods. The increase in smectites and kaolinite associated with the decrease in illite to the uppermost Pleistocene is most likely related to climate warming and also to an increase in coeval tectonic stability.

ACKNOWLEDGMENTS

We thank the Shipboard Scientific Party and the crew of the *JOIDES Resolution* for assistance with the samples and data; Isabel Nieto, Maria Dolores Dominguez, and Pascual Sánchez for their help in the laboratory; the Instrument Services of the University of Granada for the use of their analytical facilities; and the Research Group of the "Junta de Andalucía" RNM-0179. We also thank Dr. A.M. Karpoff and Dr. H. Chamley for careful revision of the manuscript. This work was supported by the CICYT of Spain under a grant for the AMB-95-1557 and AMB-95-0196 projects.

REFERENCES

Bea, F., 1996. Residence of REE, Y, Th and U in granites and crustal protoliths: implications for the chemistry of crustal melts. *J. Petrol.*, 37:521–532.

Bishop, J.K.B., 1988. The barite-opal organic carbon association in oceanic particulate matter. *Nature*, 332:341–343.

Brosse, E., 1982. Contribution à la minéralogie et à la geochimie des sédiments pélagiques profunds. Comparaisons des "black-shales" du Crétacé dans l'Atlantique central nord et des dépots du Malm et du Crétacé en Briançonnais [Ph. D. thesis]. Ecol. Nat. Sup. Mines Paris.

Chamley, H., 1989. *Clay Sedimentology:* Berlin (Springer-Verlag).

Chamley, H., Dunoyer de Segonzac, G., and Mélières, F., 1978. Clay minerals in Messinian sediments of the Mediterranean area. *In* Hsü, K.J., Montadert, L., et al., *Init. Repts. DSDP*, 42 (Pt. 1): Washington (U.S. Govt. Printing Office), 389–395.

Chamley, H., and Robert, C., 1980. Sédimentation argileuse au Tertiaire supérieur dans le domain méditerranéen. *Geol. Mediterr.*, 7:25–34

Comas, M.C., Zahn, R., Klaus, A., et al., 1996. *Proc. ODP, Init. Repts.*, 161: College Station, TX (Ocean Drilling Program).

Dunoyer de Segonzac, G., and Hoffert, M., 1973. A preliminary investigation of the clay minerals in the western Alboran basin, Site 121. *In* Ryan, W.B.F., Hsü, K.J., et al., *Init. Repts. DSDP*, 13: Washington (U.S. Govt. Printing Office),670–672.

Ercilla, G., Alonso, B., and Baraza, J., 1992. Sedimentary evolution of the northwestern Alboran Sea during the Quaternary. *Geo-Mar. Lett.*, 12:144–149.

Fisher, J.F., 1977. Smectite distribution, Leg 37 basalt. *In* Aumento, F., Melson, W.G., *Init. Repts. DSDP,* 37: Washington (U.S. Govt. Printing Office), 833–837.

Hilgen, F.J., 1991. Astronomical calibration of Gauss to Matuyama sapropels in the Mediterranean and implication for the geomagnetic polarity time scale. *Earth Planet. Sci. Lett.,* 104:226–244.

Kisch, H.J., 1991. Illite crystallinity: recommendations on sample preparation, X-ray diffraction settings, and interlaboratory samples. *J. Metamorph. Geol.,* 9:665–670.

Maillot, H., and Robert, C., 1980. Minéralogie et géochimie des sédiments crétacés cénozoiques dans l'Océan Atlantique sud (Marge africaine, dorsale medio-atlantique). *Bull. Soc. Geol. Fr.,* 22:779–789.

Martín Ramos, D., 1976. Las micas de las Cordilleras Béticas [Ph. D. thesis]. Univ. Granada.

Nesteroff, W.D., 1973. Distribution of the fine-grained sediment component in the Mediterranean. *In* Ryan, W.B.F., and Hsü, K.J., et al., *Init. Repts. DSDP,* 13 (Pt. 2): Washington U.S. Govt. Printing Office, 666–670.

Nieto, F., 1983. Las cloritas de las Cordilleras Béticas [Ph. D. thesis]. Univ. Granada.

————, 1997. Chemical composition of metapelitic chlorites: X-ray diffraction and optical property approach. *Eur. J. Mineral.,* 9:829–841.

Nieto, F., Ortega-Huertas, M., Peacor, D.R., and Arostegui, J., 1996. Evolution of the illite/smectite from early diagenesis through incipient metamorphism in sediments of the Basque-Cantabrian Basin. *Clays Clay Miner.,* 44:304–326.

Nieto, F., Ortega Huertas, M., and Velilla, N., 1989. Some crystallochemical and petrographic criteria for determining source rocks and sedimentary processes: the example of neogene deposits of the Alpujarran corridor (Betic Cordillera, SE Spain). *Clay Miner.,* 24:603–619.

Paytan, A., 1995. Marine barite, a recorder of oceanic chemistry, productivity, and circulation [Ph.D. thesis]. Scripps Inst. Oceanogr., Univ. Calif. San Diego.

Pollastro, R.M., 1985. Mineralogical and morphological evidence for the formation of illite at the expense of illite/smectite. *Clays Clay Miner.,* 33:265–274.

Shipboard Scientific Party, 1996a. Site 976. *In* Comas, M.C., Zahn, R., Klaus, A., et al., *Proc. ODP, Init. Repts.,* 161: College Station, TX (Ocean Drilling Program), 179–297.

————, 1996b. Site 977. *In* Comas, M.C., Zahn, R., Klaus, A., et al., *Proc. ODP, Init. Repts.,* 161: College Station, TX (Ocean Drilling Program), 299–353.

Singer, A., 1980. The paleoclimatic interpretation of clay minerals in soils and weathering profiles. *Earth Sci. Rev.,* 15:303–326.

Thirty, M., 1981. Sédimentation continentale et altérations associées: calcitisation, ferruginisations et silicification: les argiles plastiques du Sparnacien du Bassin de Paris. *Sci. Geol. Mem. Strasbourg,* 84.

Van der Pluijm, B.A., Lee, J.H., and Peacor, D.R., 1988. Analytical electron microscopy and the problems of potassium diffusion. *Clays Clay Miner.,* 36:498–504.

Velde, B., 1985. *Clay Minerals: A Physico-Chemical Explanation of Their Occurrence:* Amsterdam (Elsevier), Dev. Sedimentol., 40.

Weaver, C.E., and Beck, K.C., 1977. Miocene of the S.E. United States: a model for chemical sedimentation in a peri-marine environment. *Sediment. Geol.,* 17:1–234.

Weaver, C.E., and Pollard, L.D., 1973. *The Chemistry of Clay Minerals:* Amsterdam (Elsevier), Developments in Sedimentology, 15.

Zemmels, I., and Cook, H.E., 1973. X-ray mineralogy of selected samples from the sea floor of the Northeast Atlantic and Mediterranean Sea. *In* Ryan, W.B.F., and Hsü, K.J., et al., *Init. Repts. DSDP,* 13: Washington (U.S.Govt. Printing Office), 605–666.

Date of initial receipt: 7 May 1997
Date of acceptance: 3 November 1997
Ms 161SR-203

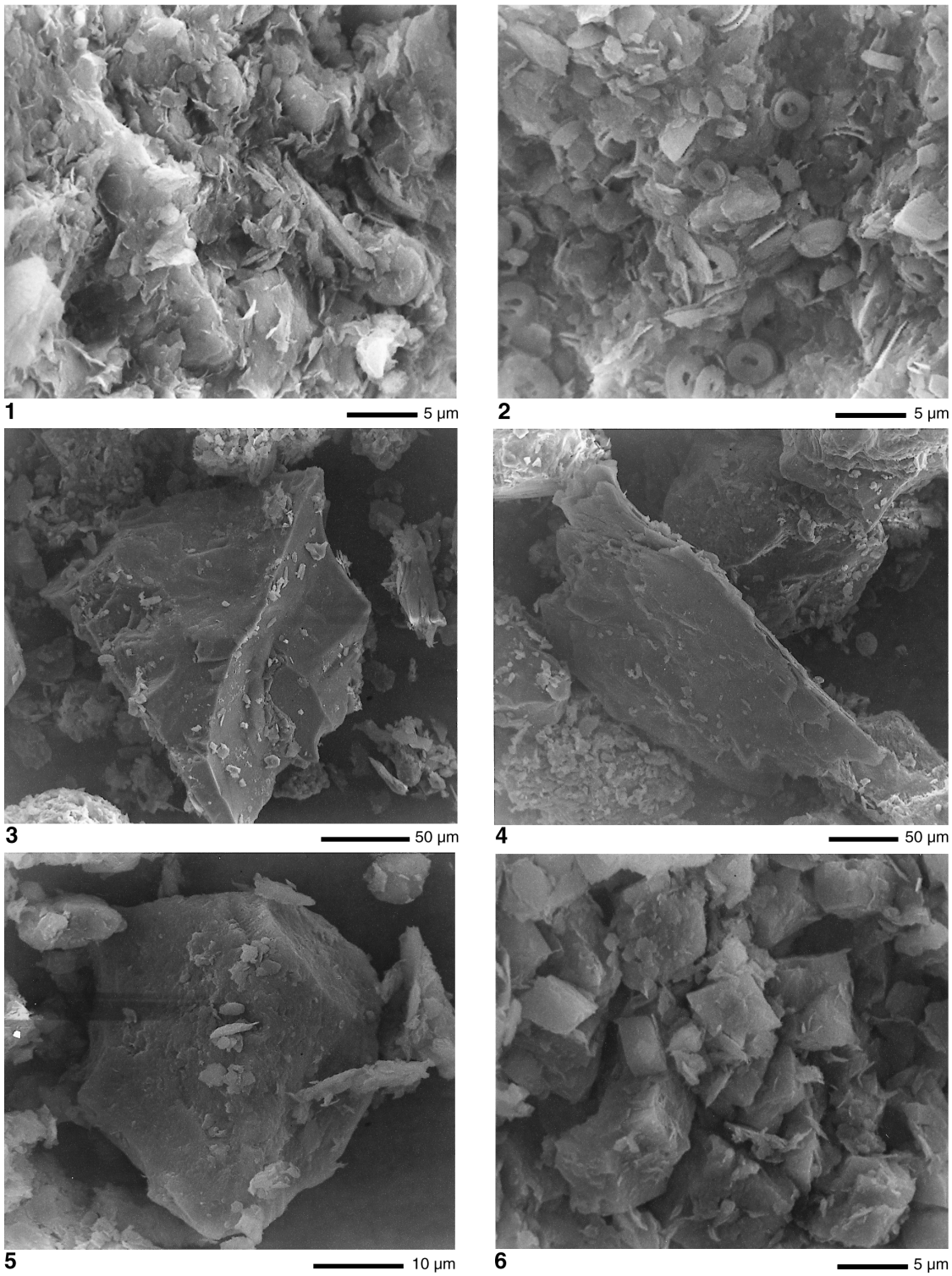

Plate 1. SEM photomicrographs from hemipelagic and resedimented facies. **1.** Clay-rich hemipelagic sediments. **2.** Calcite-rich hemipelagic sediments with abundant well-preserved nannofossils. **3.** Detrital angular quartz. **4.** Detrital mica and rounded quartz. **5.** Detrital dolomite. **6.** Euhedral dolomite crystals.